Chapter 1
Phase Behaviour, Interfacial Tension and Microstructure of Microemulsions

Thomas Sottmann and Cosima Stubenrauch

1.1 Introduction

Microemulsions are macroscopically isotropic mixtures of at least a hydrophilic, a hydrophobic and an amphiphilic component. Their thermodynamic stability and their nanostructure are two important characteristics that distinguish them from ordinary emulsions which are thermodynamically unstable. Microemulsions were first observed by Schulman [1] and Winsor [2] in the 1950s. While the former observed an optically transparent and thermodynamically stable mixture by adding alcohol, the latter induced a transition from a stable oil-rich to a stable water-rich mixture by varying the salinity. In 1959, Schulman *et al.* [3] introduced the term 'micro-emulsions' for these mixtures which were later found to be nano-structured.

The extensive research on microemulsions was prompted by two oil crises in 1973 and 1979, respectively. To optimise oil recovery, the oil reservoirs were flooded with a water–surfactant mixture. Oil entrapped in the rock pores can thus be removed easily as a microemulsion with an ultra-low interfacial tension is formed in the pores (see Section 10.2 in Chapter 10). Obviously, this method of tertiary oil recovery requires some understanding of the phase behaviour and interfacial tensions of mixtures of water/salt, crude oil and surfactant [4]. These in-depth studies were carried out in the 1970s and 1980s, yielding very precise insights into the phase behaviour of microemulsions stabilised by non-ionic [5, 6] and ionic surfactants [7–9] and mixtures thereof [10]. The influence of additives, like hydro- and lyotropic salts [11], short- and medium-chain alcohols (co-surfactant) [12] on both non-ionic [13] and ionic microemulsions [14] was also studied in detail. The most striking and relevant property of microemulsions in technical applications is the low or even ultra-low interfacial tension between the water excess phase and the oil excess phase in the presence of a microemulsion phase. The dependence of the interfacial tension on salt [15], the alcohol concentration [16] and temperature [17] as well as its interrelation with the phase behaviour [18, 19] can be regarded as well understood.

From the late 1980s onwards, the research on microemulsions turned to the understanding of the fascinating microstructure of these mixtures. Microemulsions are created by a surfactant film forming at the microscopic water/oil interface. Different methods such as NMR self-diffusion [20, 21], transmission electron microscopy (TEM) [20, 22]

and scattering techniques (small angle X-ray scattering (SAXS) [23] and small angle neutron scattering (SANS) [16, 24]) provided some of the larger pieces in the puzzle of the manifold structure of microemulsions [25]. A recent overview of the state of the art of microemulsions, which contains the basic features of microemulsions as well as their theoretical description, is given in Ref. [26].

The research on microemulsions currently concentrates on even more complex mixtures. By adding amphiphilic macromolecules the properties of microemulsions can be influenced quite significantly (see Chapter 4). If only small amounts of amphiphilic block copolymers are added to a bicontinuous microemulsion a dramatic enhancement of the solubilisation efficiency is found [27, 28]. On the other hand, the addition of hydrophobically modified (HM) polymers to droplet microemulsions leads to a bridging of swollen micelles and an increase of the low shear viscosity by several orders of magnitude [29].

Within the last 30 years, microemulsions have also become increasingly significant in industry. Besides their application in the enhanced oil recovery (see Section 10.2 in Chapter 10), they are used in cosmetics and pharmaceuticals (see Chapter 8), washing processes (see Section 10.3 in Chapter 10), chemical reactions (nano-particle synthesis (see Chapter 6)), polymerisations (see Chapter 7) and catalytic reactions (see Chapter 5). In practical applications, microemulsions are usually multicomponent mixtures for which formulation rules had to be found (see Chapter 3). Salt solutions and other polar solvents or monomers can be used as hydrophilic component. The hydrophobic component, usually referred to as oil, may be an alkane, a triglyceride, a supercritical fluid, a monomer or a mixture thereof. Industrially used amphiphiles include soaps as well as medium-chained alcohols and amphiphilic polymers, respectively, which serve as co-surfactant.

The fact that microemulsions have gained increasing importance both in basic research and in industry is reflected in the large number of publications on microemulsions. A survey of paper titles reveals that the number of papers on the subject of microemulsions increased within the last 30 years from 474 in 1976–1985 to over 2508 in 1986–1995 and to 6691 in 1996–2005.[1] The fact that microemulsions also provide the potential for numerous practical applications is mirrored in the number of patents filed on this topic. A survey of patents on microemulsions[2] shows an increase from 159 in 1976–1985 to over 805 in 1986–1995 and to 2107 in 1996–2005. In the following the basic properties of microemulsions will be presented concentrating on the close connection between the phase behaviour and the interfacial tensions as well as on the fascinating microstructure.

1.2 Phase behaviour

The primary aim of microemulsion research is to find the conditions under which the surfactant solubilises the maximum amounts of water and oil, i.e. the phase behaviour has to be studied. As the effect of pressure on the phase behaviour is (in general) rather weak [30], it is sufficient to consider the effect of the temperature. Furthermore, it has been shown that simple ternary systems consisting of water, oil and non-ionic *n*-alkyl polyglycol ethers (C_iE_j) exhibit all properties of complex and technically relevant systems [6]. Therefore, we will first describe the phase behaviour of ternary non-ionic microemulsions.

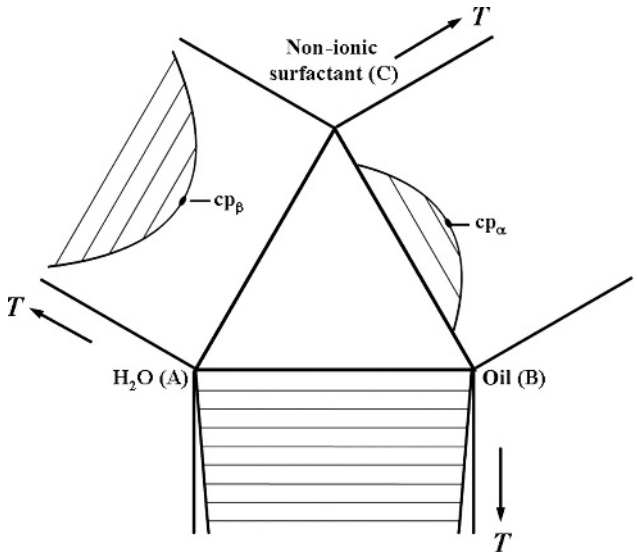

Figure 1.1 Schematic view of the phase behaviour of the three binary systems water (A)–oil (B), oil (B)–non-ionic surfactant (C), water (A)–non-ionic surfactant (C) presented as an 'unfolded' phase prism [6]. The most important features are the upper critical point cp_α of the B–C miscibility gap and the lower critical point cp_β of the binary A–C diagram. Thus, at low temperatures water is a good solvent for the non-ionic surfactant, whereas at high temperatures the surfactant becomes increasingly soluble in the oil. The thick lines represent the phase boundaries, while the thin lines represent the tie lines.

1.2.1 Microemulsions with alkyl polyglycol ethers

One successful approach to understanding the complex phase behaviour of microemulsions is to consider first the phase diagrams of the corresponding binary base systems [6]. In the case of ternary non-ionic microemulsions these are the three binary systems: water (A)–oil (B), oil (B)–non-ionic surfactant (C) and water (A)–non-ionic surfactant (C). For thermodynamic reasons, each of these systems shows a lower miscibility gap with an upper critical point. Figure 1.1 shows the unfolded phase prism with schematic diagrams of the three binary systems. The phase diagram of the binary water (A)–oil (B) system is the simplest of the three. The upper critical point of its lower miscibility gap lies well above the boiling point of the mixture, i.e. water and oil are almost immiscible between the melting and boiling point. The phase diagram of the binary oil (B)–non-ionic surfactant (C) system is almost as simple. Its upper critical point cp_α usually lies not far from the melting point of the mixture and depends on the nature of both oil and surfactant. In general, the lower the more hydrophilic the oil is and the more hydrophobic the surfactant is. The phase diagram of the binary water (A)–non-ionic surfactant (C) system is the most complex of the three. The lower miscibility gap (not shown in Fig. 1.1) lies far below the melting point of the mixture and plays no role in the following considerations. At ambient temperatures and above the critical micelle concentration (cmc) the surfactant molecules self-assemble. Additionally, concentrated and diluted liquid crystalline phases can be found [31] (not shown in Fig. 1.1). At higher temperatures most of the systems show an

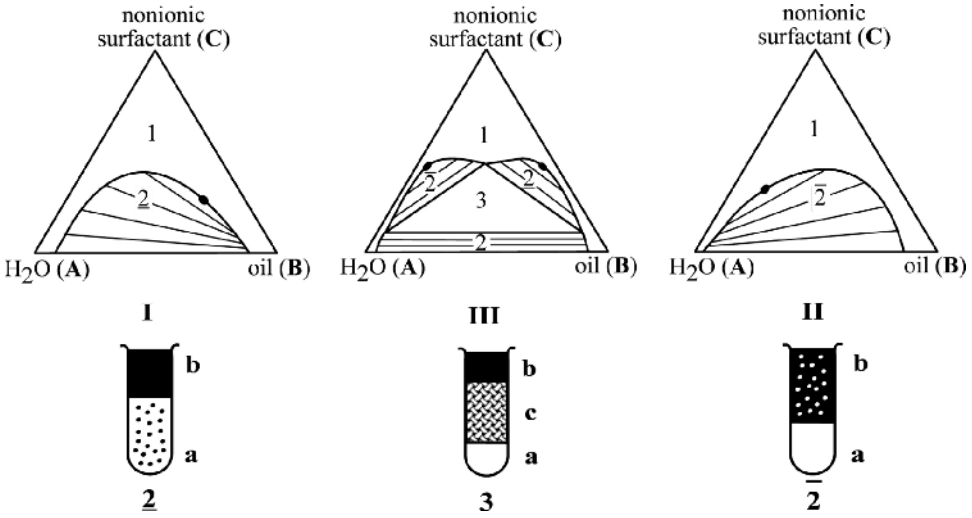

Figure 1.2 Isothermal Gibbs triangles of the system water (A)–oil (B)–non-ionic surfactant (C) at different temperatures. Increasing the temperature leads to the phase sequence $\underline{2}$–3–$\overline{2}$. A large miscibility gap can be found both at low and high temperatures. While at low temperatures a surfactant-rich water phase (a) coexists with an oil-excess phase (b), a coexistence of a surfactant-rich oil phase (b) with a water-excess phase (a) is found at high temperatures. At intermediate temperatures the phase behaviour is dominated by an extended three-phase triangle with its adjacent three two-phase regions. The test tubes illustrate the relative change in phase volumes.

additional upper (closed) miscibility gap with a lower critical point cp_β. The shape of this loop depends on the nature of the surfactant and plays an important role in the phase behaviour of the ternary system.

1.2.1.1 Phase inversion

From Fig. 1.1, it can be anticipated that the temperature-dependent phase behaviour of the ternary system is a result of the interplay between the lower miscibility gap of the B–C mixture and the upper miscibility gap of the A–C mixture. At low temperatures the non-ionic surfactant is mainly soluble in water, while it is mainly soluble in oil at high temperatures. Thus, an increase in temperature turns a non-ionic surfactant from hydrophilic into hydrophobic. Figure 1.2 shows this behaviour in the form of the related Gibbs phase triangles. At low temperatures the phase behaviour is dominated by a large miscibility gap. The negative slope of the tie lines indicates that a non-ionic surfactant-rich water phase (a) coexists with an oil-excess phase (b). This situation is denoted as $\underline{2}$ or Winsor I (see Fig. 1.2 (left)). Increasing the temperature one observes (Fig. 1.2, centre) an extended three-phase triangle with its adjacent three two-phase regions. Within the three-phase triangle (denoted as 3 or Winsor III) a surfactant-rich microemulsion (c) coexists with an excess water (a) and oil phase (b). The symmetric form of the triangle implies the solubilisation of equal amounts of water and oil. A further increase of the temperature

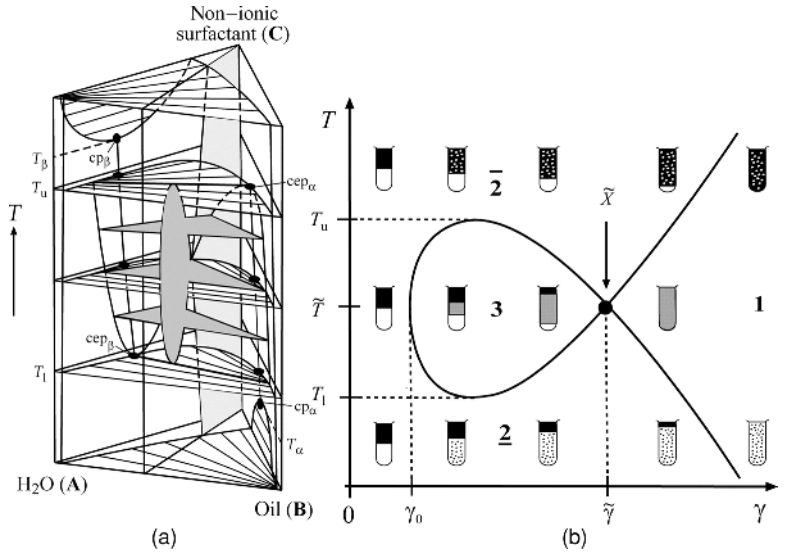

Figure 1.3 (a) Schematic phase prism of the system water–oil–non-ionic surfactant showing the temperature-dependent phase behaviour. A convenient way to study these systems is to measure the phase behaviour at constant oil/(water + oil) ratios as function of temperature T and surfactant mass fraction γ (3 phase region = dark grey, 1 phase region = light grey). (b) Schematic $T(\gamma)$-section at a constant oil/(water + oil) volume fraction of $\phi = 0.5$. Assigned are the minimal mass fraction $\tilde{\gamma}$ of surfactant needed to solubilise water and oil, the mass fraction γ_0 of surfactant which is solubilised monomerically in water and oil, the lower (T_l), upper (T_u) and mean ($\tilde{T}$) temperature of the three-phase body. Again the test tubes illustrate the relative volume of the phases.

again leads to the formation of an extended miscibility gap (see Fig. 1.2 (right)). Here, the positive slope of the tie lines indicates that a non-ionic surfactant-rich oil phase (b) coexists with a water-excess phase (a). This situation is denoted as $\overline{2}$ or Winsor II. The test tube shown below each Gibbs phase triangle illustrates the relative change in phase volumes for mixtures containing equal volumes of water and oil.

Stacking the isothermal Gibbs triangles on top of each other results in a phase prism (see Fig. 1.3(a)), which represents the temperature-dependent phase behaviour of ternary water–oil–non-ionic surfactant systems. As discussed above, non-ionic surfactants mainly dissolve in the aqueous phase at low temperatures ($\underline{2}$). Increasing the temperature one observes that this surfactant-rich water phase splits into two phases (a) and (c) at the temperature T_l of the lower critical endpoint cep_β, i.e. the three-phase body appears. Subsequently, the lower water-rich phase (a) moves towards the water corner, while the surfactant-rich middle phase (c) moves towards the oil corner of the phase prism. At the temperature T_u of the upper critical endpoint cep_α a surfactant-rich oil phase is formed by the combination of the two phases (c) and (b) and the three-phase body disappears. Each point in such a phase prism is unambiguously defined by the temperature T and two composition variables. It has proved useful [6] to choose the mass fraction of the oil in the

mixture of water and oil

$$\alpha = \frac{m_B}{m_A + m_B} \tag{1.1}$$

and that of the surfactant in the mixture of all three components

$$\gamma = \frac{m_C}{m_A + m_B + m_C}. \tag{1.2}$$

Knowing the densities of the components for calculating the volumes one can also use the volume fractions ϕ and ϕ_C, respectively. A simple and extremely useful procedure to obtain an overview of the phases occurring in such a phase prism is to measure the phase diagram at a constant oil/water ratio as a function of the temperature T and the surfactant mass fraction γ ($T(\gamma)$-section). Such a section through the phase prism is highlighted in Fig. 1.3(a) (3 phase region = dark grey, 1 phase region = light grey) and shown schematically in Fig. 1.3(b). It permits easily to determine the *phase inversion temperature* (PIT), at which the hydrophilic–lipophilic balance (HLB) is achieved.

Figure 1.3(b) shows such a $T(\gamma)$-section at a constant oil/(water + oil) volume fraction of $\phi = 0.5$. As can be seen, the phase boundaries resemble the shape of a fish. Starting with the binary water–oil system, two phases, namely a pure water phase and a pure oil phase, coexist over the entire experimentally accessible temperature range. Small amounts of added surfactant molecules dissolve monomerically in the two phases. Being amphiphilic, the surfactant molecules preferentially adsorb at the macroscopic interface. At a mass fraction γ_0 both excess phases and the macroscopic interface are saturated with the surfactant molecules and the amphiphilic molecules are forced into the microscopic water/oil interface leading to topologically ordered interfacial films in solutions, i.e. the 'real' microemulsions. Looking at these mixtures microscopically, we find at low temperatures an amphiphilic film that forms oil-swollen micelles in a continuous water phase (a). This oil-in-water (o/w) microemulsion coexists with an oil-excess phase (b) ($\underline{2}$). At high temperatures the inverted situation ($\overline{2}$) is found. Here, a water excess phase (a) coexists with a water-in-oil (w/o) microemulsion in which the amphiphilic film forms water-swollen micelles in a continuous oil phase (b). At intermediate temperatures the surfactant is almost equally soluble in both solvents and a locally planar amphiphilic film is formed. Here, three phases (3), i.e. a surfactant-rich bicontinuously structured (for details see below) phase (c), an excess oil and water phase coexist. Microscopically, the observed trend of the phase behaviour from $\underline{2}$ over 3 to $\overline{2}$ with increasing temperature can be attributed to a gradual change of the mean curvature H of the amphiphilic film [25, 32]. While at low temperatures the film is curved around the oil ($H > 0$) it curves around water at high temperatures ($H < 0$) (see Section 1.4, Fig. 1.18).

Considering now the variation of the phase behaviour with increasing mass fraction γ of surfactant one can see that the volume of the respective microemulsion phase increases (see test tubes in Fig. 1.3(b)) until the excess phases vanish and a one-phase microemulsion is found. The optimal state of the system is the so-called $\tilde{X}$-point where the three-phase body meets the one-phase region. It defines both the minimum mass fraction $\tilde{\gamma}$ of surfactant needed to solubilise water and oil, i.e. the efficiency of the surfactant, as well as the corresponding temperature $\tilde{T}$, which is a measure of the PIT.

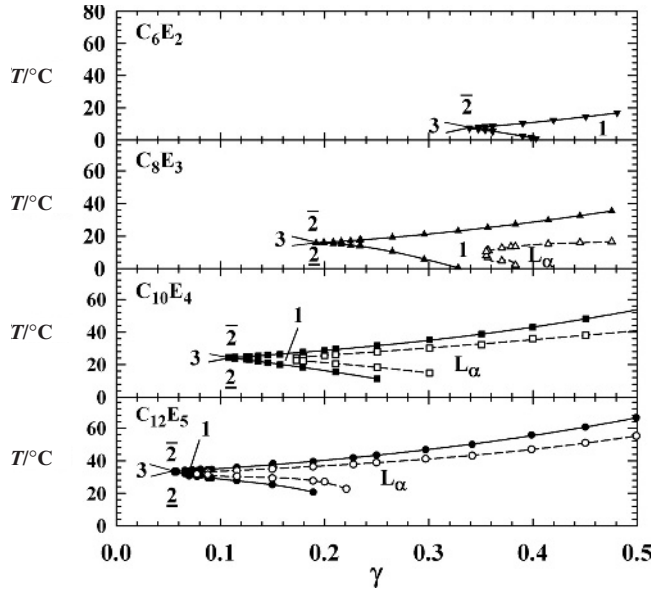

Figure 1.4 $T(\gamma)$-sections through the phase prism of the systems H_2O–*n*-octane–C_6E_2, C_8E_3, $C_{10}E_4$ and $C_{12}E_5$ at an oil/(water + oil) volume fraction of $\phi = 0.5$. In order to determine the respective $\tilde{X}$-point the phase boundaries are measured only for surfactant mass fractions $\gamma > \tilde{\gamma}$. An increase of both the hydrophobic chain length *i* and the size of the hydrophilic head group *j* shifts the $\tilde{X}$-point to lower values of $\tilde{\gamma}$, i.e. the efficiency increases. Simultaneously the stability range of the bicontinuous one phase microemulsion shrinks dramatically due to the increased extension of the lamellar mesophase (L_α). (From Ref. [26], reprinted with permission of Elsevier.)

1.2.1.2 Efficiency

One of the central questions of microemulsion formulation has been, and still is, the quest for high efficiency, i.e. finding microemulsions in which a minimum amount of surfactant is necessary for solubilising oil in water or vice versa. A rapid method for quantifying the efficiency of a system is to determine the $\tilde{X}$-point by recording a $T(\gamma)$-section at an oil/(water + oil) volume fraction $\phi = 0.5$. In this fashion the optimal state ($\tilde{X}$-point) can be determined extrapolating the phase boundaries from $\underline{2}$ to 1 (turbid to clear) and 1 to $\overline{2}$ (clear to turbid), which makes the exact determination of the three-phase region dispensable. In Fig. 1.4, it is demonstrated in which way the $\tilde{X}$-point and, consequently, the one-phase microemulsion region ($\gamma > \tilde{\gamma}$) are influenced by the chain length of the surfactant [26]. The figure shows the $T(\gamma)$-section of four H_2O–*n*-octane–*n*-alkyl polyglycol ether (C_iE_j) systems at an oil/(water + oil) volume fraction of $\phi = 0.5$. Starting with the H_2O–*n*-octane–C_6E_2 system (Fig. 1.4, top) it can be seen that a surfactant mass fraction of $\tilde{\gamma} = 0.334$ is needed for the solubilisation of equal volumes of water and *n*-octane. Using the surfactant C_8E_3 instead of C_6E_2 only 19 wt.% of surfactant is needed to solubilise water and *n*-octane. A further increase of the chain length of the surfactant to $C_{10}E_4$ and $C_{12}E_5$ shifts the $\tilde{X}$-point to $\tilde{\gamma} = 0.099$ and $\tilde{\gamma} = 0.048$, respectively. Thus, enlarging both the alkyl chain *i* and the head group size *j* (number of ethylene oxide groups) of the surfactant from

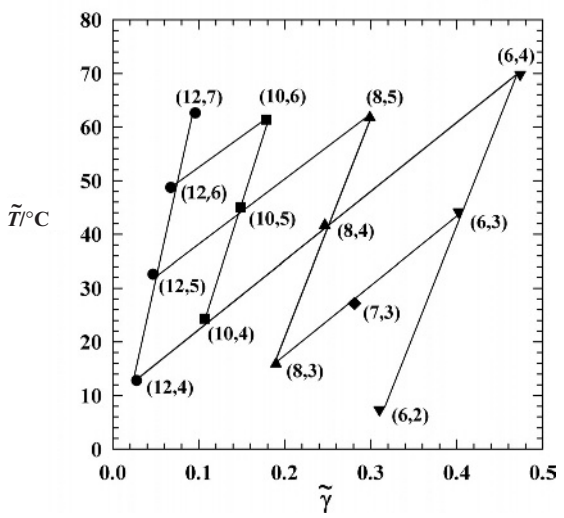

Figure 1.5 $\tilde{X}$-points of the systems H_2O–*n*-octane–C_iE_j at an oil/(water + oil) volume fraction of $\phi = 0.5$ [34]. The individual systems are characterised by the (*i*, *j*) pairs. While an increase of the hydrophobic chain length *i* leads mainly to a decrease of $\tilde{\gamma}$, an increase of the number of oxyethylene groups *j* increases mainly $\tilde{T}$. (From Ref. [34], reprinted with permission of the Royal Society of Chemistry.)

C_6E_2 to $C_{12}E_5$ leads to an enormous increase in efficiency. This increase in efficiency is a result of the increasing amphiphilicity of the surfactant molecules forcing them into the microscopic water/oil interface.

All four systems show the phase sequence characteristic of non-ionic microemulsions, namely $\underline{2} \rightarrow 3 \rightarrow \overline{2}$ at intermediate and $\underline{2} \rightarrow 1 \rightarrow \overline{2}$ at larger surfactant mass fractions. However, the lamellar liquid crystalline phase L_α (surrounded by a two-phase coexistence region, not shown), which is not present in the C_6E_2 system, occurs in the C_8E_3 system where it is embedded in the one-phase region of the microemulsion. Increasing the amphiphilicity of the surfactant even further leads to an extension of the L_α phase that nearly covers the entire one-phase region and thus limits the existence of the one-phase bicontinuous microemulsion to a very small region. As these liquid crystalline phases are often highly viscous and thus tend to complicate the handling of water–oil-surfactant systems their formation is undesirable in technical applications. An alternative and new road to the formulation of highly efficient microemulsion is the addition of small amounts of amphiphilic block copolymers to medium-efficient microemulsions [27, 33] (see Chapter 4).

In general, the $\tilde{X}$-point gives the efficiency of the surfactant and the PIT provides an excellent criterion for choosing the appropriate surfactant for the formulation in question. In Fig. 1.5, a synopsis of the $\tilde{X}$-points of 14 different H_2O–*n*-octane–C_iE_j systems at an oil/(water + oil) volume fraction of $\phi = 0.5$ is shown in a $\tilde{T}(\tilde{\gamma})$ plot [34]. The hydrophobic chain length *i* is varied between 6 and 12, the number of ethylene oxide groups *j* between 2 and 7. An increase of the hydrophobic chain length *i* renders the surfactant more hydrophobic. Thus, the $\tilde{X}$-point shifts to lower temperatures. Concomitantly, $\tilde{\gamma}$ decreases strongly, i.e. the surfactant becomes more efficient. An increasing number of ethylene oxide

groups j shifts the $\tilde{X}$-point to higher temperatures due to an increasing hydrophilicity of the surfactant and $\tilde{\gamma}$ increases slightly. Furthermore, the whole grid of the $\tilde{X}$-points varies systematically with the chain length k of the n-alkane (not shown in Fig. 1.5 for the sake of clarity). Kahlweit *et al.* found [11] that with increasing k the $\tilde{X}$-point shifts to higher temperatures and $\tilde{\gamma}$ increases, i.e. the surfactant becomes less efficient. Recently, analogous trends of the $\tilde{X}$-point with k have been observed for both polymerisable n-alkyl methacrylates [35] and triglycerides [36].

1.2.1.3 Monomeric solubility

In one-phase microemulsions the surfactant molecules partition between the microscopic water/oil interface and the microemulsion sub-phases (e.g. in swollen micelles or bicontinuous oil- and water-rich domains) in which they are dissolved monomerically. They also dissolve monomerically in coexisting excess phases and adsorb at the macroscopic interfaces between the phases. The significance of this fact is that these parts of the surfactant are not available for the micro-emulsification of water and oil. Thus, for technical applications surfactants with high amphiphilicity but small monomeric solubilities in both solvents are desirable.

The monomeric solubility of the surfactant in the water $\gamma_{\mathrm{Cmon,a}}$ can be easily determined from surface tension measurements [37]. An interesting method to obtain $\gamma_{\mathrm{Cmon,b}}$ is provided by the macroscopic phase behaviour through the determination of the mass fraction of surfactant γ_0 (see Fig. 1.3), i.e. the monomerically dissolved surfactant in both excess phases. Therefore, the volume fraction of the middle phase V_c/V has to be measured as a function of the mass fraction of surfactant γ at a constant $\phi = 0.5$ and the mean temperature $\tilde{T}$ of the three-phase body [34, 38, 39]. Plotting V_c/V versus γ yields γ_0 at $V_\mathrm{c}/V = 0$ and $\tilde{\gamma}$ at $V_\mathrm{c}/V = 1$. Then the monomeric solubility in the oil is calculated from

$$\gamma_{\mathrm{Cmon,b}} = \frac{\gamma_0 + \gamma_{\mathrm{Cmon,a}}(\alpha(1-\gamma_0)-1)}{\gamma_0 + \alpha(1-\gamma_0) - \gamma_{\mathrm{Cmon,a}}}. \tag{1.3}$$

Figure 1.6 shows the monomeric solubility $\gamma_{\mathrm{Cmon,b}}$ in n-octane calculated according to Eq. (1.3) at the respective mean temperature $\tilde{T}$ of the three-phase body [34]. For the calculations the monomeric solubility $\gamma_{\mathrm{Cmon,a}}$ in water was set equal to 0.03, 0.02, 0.01, 0.006 and 0.002 for C_6E_2, C_6E_3, C_6E_4, C_7E_3 and C_8E_j, respectively. For longer chain surfactants $\gamma_{\mathrm{Cmon,a}} < 0.001$ was neglected [40, 41]. For the sake of visual clarity, a grid of lines was drawn through the data points at constant i and j to even out the experimental error.

As can be seen, the $\tilde{T}(\gamma_{\mathrm{Cmon,b}})$ plot shows the same pattern as the $\tilde{T}(\tilde{\gamma})$ plot, i.e. the monomeric solubility $\gamma_{\mathrm{Cmon,b}}$ in n-octane decreases with increasing hydrophobic chain length i and increases slightly with increasing number of ethylene oxide groups j. These findings suggest that both monomeric solubilities are correlated with the efficiency of the surfactant to solubilise water and oil. Having the monomeric solubility of the surfactants in both water and oil at hand the mass fraction γ_i of the surfactant molecules which reside

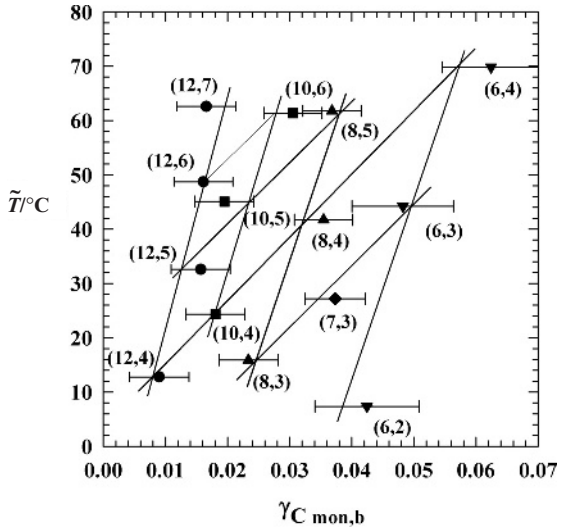

Figure 1.6 Monomeric solubility $\gamma_{Cmon,b}$ of 14 different surfactants in *n*-octane at the mean temperature $\tilde{T}$ obtained from the determination of γ_0 (see Fig. 1.3) [34]. Note the similar patterns of the $\tilde{T}(\gamma_{Cmon,b})$ plot and the $\tilde{T}(\tilde{\gamma})$ plot (see Fig. 1.5), respectively. (From Ref. [34], reprinted with permission of the Royal Society of Chemistry.)

at the microscopic water/oil interface can be calculated according to

$$\gamma_i = \gamma - \frac{w_A \gamma_{Cmon,a}}{1 - \gamma_{Cmon,a}} - \frac{w_B \gamma_{Cmon,b}}{1 - \gamma_{Cmon,b}}, \tag{1.4}$$

where w_A and w_B are the weight fractions of water and oil, respectively. The parameter γ_i is a measure for the size of the specific area of the interface S/V ($S/V \sim \gamma_i$), for the characteristic length ξ ($\xi \sim \gamma_i^{-1}$) of the structures [42–44], and for the interfacial tension σ_{ab}($\sigma_{ab} \sim \gamma_i^2$) between water- and oil-rich phases [45, 46] (for details see Sections 1.3 and 1.4).

The facts presented so far show that the general phase behaviour, the location of the three-phase body (i.e. $\tilde{\gamma}$, $\tilde{T}$(PIT)) and the monomeric solubilities ($\gamma_{Cmon,a}$, $\gamma_{Cmon,b}$) depend sensitively but systematically on the chemical nature of the components. Furthermore, the striking similarities that many systems share suggest that, as in the corresponding state description for real gases, suitable parameters exist which scale the phase behaviour of all microemulsions. Systematic measurements of the extension of the three-phase body identified $\tilde{\gamma}(\phi = 0.50)$, T_l and T_u as the relevant parameters for a corresponding state description of microemulsions [47]. These parameters also determine the phase behaviour far on the water- and oil-rich side of the phase prism which is particularly interesting for technical applications.

1.2.1.4 Water- and oil-rich microemulsions

The phase behaviour of water-rich and oil-rich microemulsions can be studied most conveniently by considering vertical sections through the phase prism at a constant surfactant/(water + surfactant) mass fraction

$$\gamma_a = \frac{m_C}{m_A + m_C} \tag{1.5}$$

and a constant surfactant/(oil + surfactant) mass fraction

$$\gamma_b = \frac{m_C}{m_B + m_C}, \tag{1.6}$$

respectively. Starting from the binary systems A–C or B–C, the temperature-dependent phase behaviour is measured as a function of the mass fraction of oil w_B or water w_A, respectively. A schematic drawing of $T(w_B)$- and $T(w_A)$-sections performed at constant mass fractions γ_a and γ_b, respectively, is seen in Fig. 1.7(a). The variation of the phase behaviour in these sections is discussed by means of the system H_2O–*n*-octane–$C_{10}E_5$. Figure 1.7(b) shows the section on the water-rich side ($T(w_B)$ at $\gamma_a = 0.10$), while the corresponding section ($T(w_A)$ at $\gamma_b = 0.10$) on the oil-rich side of the phase prism is shown in Fig. 1.7(c).

Looking first of all at the phase boundaries of the $T(w_B)$-section one observes that the $1 \rightarrow \overline{2}$ phase boundary starts at $w_b = 0$ near the critical point of the miscibility gap of the binary water–$C_{10}E_5$ system. Upon the addition of *n*-octane this near-critical boundary descends steeply and runs through a minimum as the weight fraction of oil w_b is increased further. Simultaneously, the $\underline{2} \rightarrow 1$ phase boundary ascends monotonically with increasing w_B. This phase boundary indicates, for a given temperature, the maximum amount of oil that can be solubilised in a one-phase oil-in-water (o/w) microemulsion and is thus called the *emulsification failure boundary* (*efb*). With increasing temperature the capability of the surfactant to solubilise oil is strongly increased. Close to the lower critical endpoint temperature T_l the one-phase region closes like a funnel. It terminates at the intersection of the lower oil emulsification failure and the upper near-critical phase boundary.

At the oil-rich side, the phase behaviour is inverted temperature-wise as can be seen in the $T(w_A)$-section provided in Fig. 1.7(c). Thus, the near-critical phase boundary $\underline{2} \rightarrow 1$ starts at low temperatures from the lower *n*-octane–$C_{10}E_5$ miscibility gap (below $<0^\circ$C) and ascends steeply upon the addition of water. With increasing w_A, this boundary runs through a maximum and then decreases down to the upper critical endpoint temperature T_u. The emulsification failure boundary $1 \rightarrow \overline{2}$ starts at high temperatures and low values of w_A, which means that only small amounts of water can be solubilised in a water-in-oil (w/o) microemulsion at temperatures far above the phase inversion. Increasing amounts of water can be solubilised by decreasing the temperature, i.e. by approaching the phase inversion. At T_u the *efb* intersects the near-critical phase boundary and the funnel-shaped one-phase region closes.

From the above considerations, it can be concluded that $T(w_B)$- and $T(w_A)$-sections provide an easy method to determine the location of emulsification failure boundaries which are of particular interest if the optimal formulation for an industrial application has to be found. Furthermore, these sections yield the lower and upper temperature of

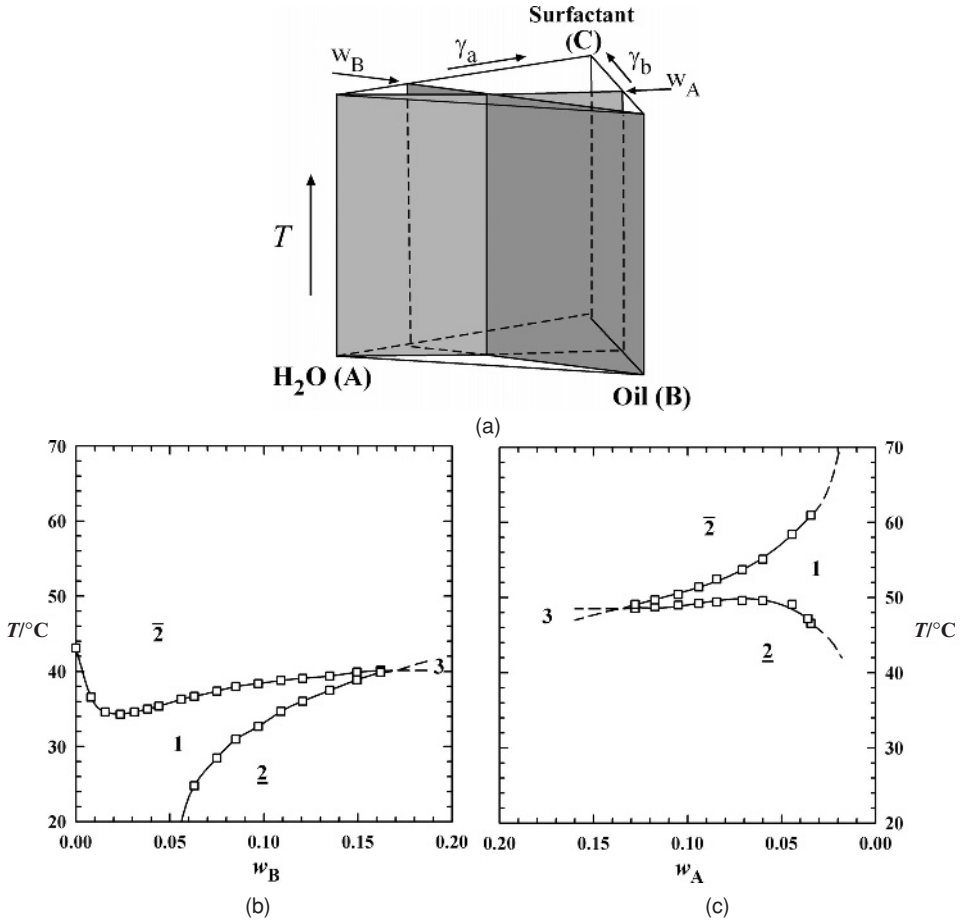

Figure 1.7 Vertical sections $T(w_B)$ and $T(w_A)$ through the phase prism which start at the binary water–surfactant ($w_B = 0$) and the binary oil–surfactant ($w_A = 0$) corner, respectively. These sections have been proven useful to study the phase behaviour of water- and oil-rich microemulsions. (a) Schematic view of the sections $T(w_B)$ and $T(w_A)$ performed at a constant surfactant/(water + surfactant) mass fraction γ_a and at a constant surfactant/(oil + surfactant) mass fraction γ_b, respectively. (b) $T(w_B)$ section through the phase prism of the system H_2O–*n*-octane–$C_{10}E_5$ at $\gamma_a = 0.10$. Starting from the binary system with increasing mass fraction of oil w_B, the oil emulsification boundary ($\underline{2} \rightarrow 1$) ascends, while the near-critical phase boundary ($1 \rightarrow \overline{2}$) descends. (c) $T(w_A)$ section through the phase prism of the system H_2O–*n*-octane–$C_{10}E_5$ at $\gamma_b = 0.10$. The inverse temperature behaviour is found on the oil-rich side: With increasing fraction of water w_A the water emulsification boundary ($1 \rightarrow \overline{2}$) descends, whereas the near-critical phase boundary ($\underline{2} \rightarrow 1$) ascends.

the three-phase body (T_l and T_u) and allow distinguishing between weak and strong surfactants if one considers the shapes of the near-critical phase boundaries [41]. While for weak surfactant systems the boundary decreases down to T_l (water-rich side) and increases up to T_u (oil-rich side), in strong surfactant systems the near-critical phase boundary has a minimum (water-rich side) and a maximum (oil-rich side), respectively. These extrema

originate from additional two-phase regions in the form of closed loops appearing at temperatures below T_l and above T_u in the Gibbs triangle [37, 41, 48, 49]. The origin of the loops (the separation of a micellar phase into two phases which become homogeneous again upon swelling with a solute) was not understood for a long time. Recently, Safran *et al.* attributed the origin of the loops to the demixing of a connected network of swollen cylindrical micelles into a dense connected network in equilibrium with a dilute phase [50–52]. This description also explains why the loops appear only in strongly structured and not in weakly structured microemulsions.

Having discussed the general phase behaviour of microemulsions by studying simple ternary non-ionic systems of the type the water–*n*-alkane–*n*-alkyl polyglycol ether (C_iE_j) we will now apply this knowledge to more complex systems relevant in technical applications. It will be shown that the insight gained by studying the temperature dependence of ternary non-ionic microemulsions can easily be adapted to systems containing technical-grade non-ionic surfactants, *n*-alkylpolyglucosides, ionic surfactants as well as mixtures of non-ionic and ionic surfactants.

1.2.2 Microemulsions with technical-grade non-ionic surfactants

In industrial applications, technical-grade surfactants which are usually mixtures of homologues and (or) isomers are used instead of pure surfactants. Common non-ionic technical-grade surfactants are ethoxylated alcohols or ethoxylated alkyl phenols. In contrast to the pure C_iE_j surfactants, which were discussed above, the technical-grade surfactants have a broad distribution of the ethoxylation degree and a residual amount of non-reacted alcohol. However, the chain length of the alcohol is rather narrowly distributed. Several studies on microemulsions formulated with technical-grade surfactants have shown that surfactant blends can be treated as a single (pseudo) component [39, 53–55]. Thus, the phase behaviour of such a pseudo-ternary system can also be characterised by $T(\gamma)$-sections through the phase prism as was described above.

In order to show the effect of technical-grade surfactants on the phase behaviour of microemulsions, $T(\gamma)$-sections of the systems H_2O–*n*-octane–$C_{12}E_6$ and the technical grade analogue DA-6 (dodecyl-alcohol-6) are shown for comparison in Fig. 1.8 [56]. As can be seen, the $C_{12}E_6$ system shows the well-known phase behaviour of ternary non-ionic microemulsions with a horizontal three-phase region that touches the horizontal one-phase region at the $\tilde{X}$-point. On the other hand, the phase boundaries of the system containing the technical-grade surfactant are strongly distorted, especially at low γ. Despite this distortion the two systems behave in a similar way. Both systems are rather efficient and show an extended L_α phase within the one-phase region. However, the technical-grade DA-6 system solubilises water and *n*-octane slightly more efficiently than the pure $C_{12}E_6$ surfactant.

The distortion of the phase boundaries in the system with the technical-grade surfactant can be explained with the broad distribution of the ethoxylation degree of DA-6 and the resulting different monomeric solubilities of every specific homologue in water $\gamma_{Cmon,a}$ and oil $\gamma_{Cmon,b}$. Taking into account only $\gamma_{Cmon,b}$ (because $\gamma_{Cmon,a} << \gamma_{Cmon,b}$ for non-ionic surfactants (see Fig. 1.6)), the lower ethoxylated, more hydrophobic homologues of the surfactant DA-6 tend to dissolve in the oil-excess or sub-phase (e.g. in oil-swollen

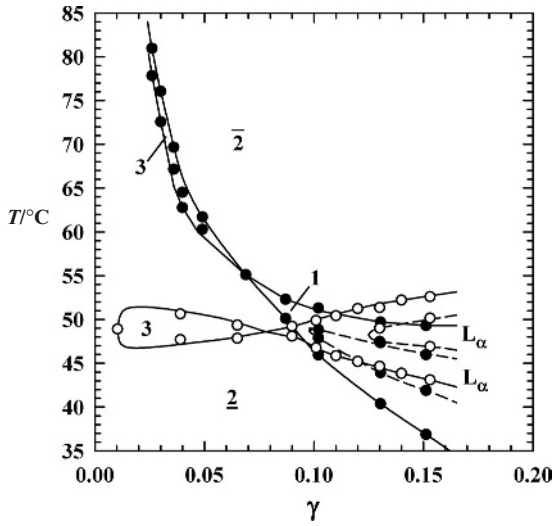

Figure 1.8 $T(\gamma)$-section through the phase prism of the systems H_2O–*n*-octane–$C_{12}E_6$ and the technical grade analogue DA-6 at an oil/(water + oil) volume fraction of $\phi = 0.5$. In contrast to the horizontal fish-type phase diagram of the $C_{12}E_6$ system the phase boundaries of the technical-grade surfactant system are distorted towards low γ. This effect is due to the broad distribution of the ethoxylation degrees of DA-6 and the higher monomeric oil solubility of the hydrophobic homologues in *n*-octane. (Figure redrawn with data from Ref. [56].)

micelles or bicontinuous oil-rich domains). Thus, the remaining surfactant mixture in the amphiphilic film is effectively more hydrophilic than the base-surfactant DA-6. Decreasing the surfactant mass fraction γ by adding water and oil one extracts increasing amounts of the more hydrophobic fractions of the surfactant DA-6 from the amphiphilic film, which accordingly becomes increasingly hydrophilic. Following the properties of ternary non-ionic microemulsions (see Fig. 1.5), the phase behaviour shifts to higher temperatures with decreasing γ, explaining the large distortion of the phase boundaries, i.e. an increasing HLB with decreasing γ. The distortion of the phase boundaries can also be discussed in terms of the mean curvature H of the amphiphilic film (see Section 1.4, Fig. 1.18). Upon decreasing γ, the fraction of surfactant molecules with large head groups increases within the film and leads to an amphiphilic film which is increasingly curved around the oil. Accordingly, within the technical-grade surfactant systems the mean curvature H of the amphiphilic film as well as the phase behaviour both depend not only on the temperature, but also on the composition of the film. In the following the dependence of the phase behaviour on the composition of the mixed amphiphilic film will be discussed in more detail.

1.2.3 Microemulsions with alkylpolyglucosides

The formulation of non-toxic, biodegradable microemulsions is of enormous importance in the cosmetic and pharmaceutical industries. One class of biodegradable surfactants which can be used to formulate such non-toxic microemulsions are the non-ionic

alkylpolyglucosides (C_mG_n, where m is the number of carbons within the hydrophobic chain and n is the number of glucose units) [57]. However, having six hydroxyl groups in one glucose unit these sugar surfactants are usually rather hydrophilic. Thus, hydrophobic amphiphiles, like alcohols [58–61] or hydrophobic C_iE_j-surfactant [62] have to be added to these rather hydrophilic C_mG_n-surfactants to formulate microemulsions. Furthermore, the weak temperature dependence of the strong hydration of the hydroxyl groups causes the rather weak temperature sensitivity of the C_mG_n-microemulsions. Thus, temperature is not the appropriate parameter to tune the mean curvature of the amphiphilic film and with it the phase behaviour of the system. Instead, the mixing of two surfactants of different hydrophilicity is the appropriate method to drive the quaternary system through the phase inversion.

In general, the phase behaviour of such a quaternary system containing H_2O, oil, a hydrophilic C_mG_n- and a hydrophobic co-surfactant is rather complex. At constant temperature and pressure it has to be represented within a phase tetrahedron (see Fig. 1.9(a)). As for the ternary temperature-sensitive microemulsions (see Fig. 1.1) an insight into the phase behaviour of a quaternary system can be gained by considering the phase diagrams of the corresponding ternary base systems. In the following the phase behaviour of the quaternary system H_2O–*n*-octane–*n*-octyl-β-D-glucopyranoside (β-C_8G_1)–1-octanol (C_8E_0) system will be discussed as an example. Systematic studies have shown that all ternary base systems (= faces of the phase tetrahedron) show extensive miscibility gaps at $T = 25^\circ$C [61]. Here, the phase behaviour of the two-side systems H_2O–*n*-octane–β-C_8G_1 and H_2O–*n*-octane–C_8E_0 are of major interest. Within the former system the β-C_8G_1 molecules prefer the water phase, i.e. a $\underline{2}$ miscibility gap is formed. In contrast, the latter system shows a $\overline{2}$ behaviour, i.e. the C_8E_0 molecules reside mainly in the oil phase. Since on top of this there is the demixing tendency of the third ternary-side system H_2O–C_8E_0–β-C_8G_1 the formation of a three-phase region is induced inside the phase tetrahedron. Figure 1.9(a) illustrates this situation schematically by means of a $w_D(w_C)$-section through the phase tetrahedron at a constant oil/(water + oil) fraction. As can be seen, a typical fish-type phase diagram is found if the ratio of co-surfactant (D) in the surfactant (C) plus co-surfactant (D) mixture

$$\delta = \frac{m_D}{m_C + m_D} \tag{1.7}$$

is varied. The monomeric solubilities of surfactant and co-surfactant in water and oil, i.e. $\gamma_{Cmon,a}$, $\gamma_{Dmon,a}$, $\gamma_{Cmon,b}$ and $\gamma_{Dmon,b}$ as well as the HLB-plane (HLB = hydrophilic–lipophilic–balance) are also shown in Fig. 1.9(a). As has already been mentioned above, the HLB-plane indicates the compositions at which the mean curvature H of the amphiphilic film is zero, i.e. the system is driven through the phase inversion. Thus, the three-phase triangle (shown in dark grey) has to lie in the HLB-plane.

In order to determine $w_D(w_C)$-sections through the phase tetrahedron experimentally a sample containing the desired amounts of water, oil and surfactant has to be titrated with the co-surfactant. Figure 1.9(b) shows such a $w_D(w_C)$-section for the H_2O–*n*-octane–*n*-octyl-β-D-glucopyranoside (β-C_8G_1)–1-octanol (C_8E_0) system at $\phi = 0.50$ and $T = 25^\circ$C [61]. As can be seen, the phase sequence $\underline{2}$–3–$\overline{2}$ is found with increasing 1-octanol content at low mass fractions of β-C_8G_1, while at higher mass fractions of β-C_8G_1, the $\underline{2}$–1–$\overline{2}$

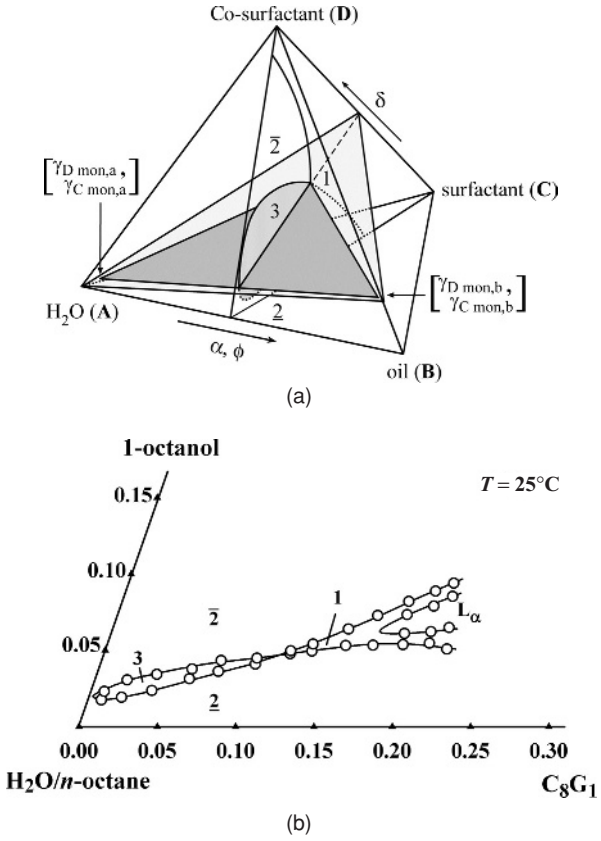

Figure 1.9 (a) Schematic phase tetrahedron of a quaternary water (A)–oil (B)–surfactant (C)–co-surfactant (D) system at constant temperature and pressure [39]. Shown is a section at a constant oil/(water + oil) ratio and the HLB-plane (HLB = hydrophilic–lipophilic–balance). The latter indicates the compositions at which the curvature of the amphiphilic film is zero. Note that the three-phase triangle (shown in dark grey) lies in the HLB-plane. (b) Section through the phase tetrahedron for the quaternary system H_2O–*n*-octane–*n*-octyl-β-D-glucopyranoside (C_8G_1)–1-octanol (C_8E_0) at a constant oil/(water + oil) volume fraction of $\phi = 0.5$ and $T = 25°C$ [61]. The system is driven through the phase inversion by adding C_8E_0. (Figure redrawn with data from Ref. [61].)

sequence is observed. For even higher mass fractions a lamellar phase appears. In these quaternary systems the location of the $\tilde{X}$-point is typically given by the ratio δ and the overall mass fraction surfactant (i.e. surfactant plus co-surfactant)

$$\gamma = \frac{m_C + m_D}{m_A + m_B + m_C + m_D}. \tag{1.8}$$

The $\tilde{X}$-point for the system under consideration lies at $\tilde{\delta} = 0.276$ and $\tilde{\gamma} = 0.161$, which shows that the surfactant/co-surfactant mixture β-C_8G_1/C_8E_0 solubilises water and *n*-octane with a medium efficiency. Comparing the $w_D(w_C)$-section performed through the phase tetrahedron with the $T(\gamma)$-section through the phase prism (see, e.g. Fig. 1.3) one

sees that a fish-type phase diagram is found in both quaternary temperature-insensitive and ternary temperature-sensitive microemulsions. Thus, the temperature T may simply be replaced by the fraction δ of co-surfactant in the mixture of surfactant and co-surfactant. However, it turned out that a quantitative description of the quaternary temperature-insensitive systems can only be obtained if the composition of the amphiphilic film

$$\delta_i = \frac{m_{D,i}}{m_{D,i} + m_{C,i}} \tag{1.9}$$

is used instead of δ, where $m_{C,i}$ and $m_{D,i}$ correspond to the mass of surfactant and co-surfactant molecules residing in the mixed amphiphilic film. To determine δ_i the monomeric solubilities (see Fig. 1.6) of 1-octanol in *n*-octane and β-C_8G_1 in H_2O have to be known, while the solubilites of 1-octanol in H_2O and β-C_8G_1 in *n*-octane can be neglected. The former can be determined individually from the phase behaviour applying the analysis of Kunieda and co-workers [63, 64].

The phase behaviour of the quaternary system can thus be tuned by varying the composition of the amphiphilic film δ_i. Starting from the ternary system H_2O–*n*-octane–β-C_8G_1 at $\phi = 0.50$ and at a mass fraction $\gamma = 0.10$ of β-C_8G_1 an oil-in-water (o/w) microemulsion forms that coexists with an excess oil phase ($\underline{2}$). As one adds the 1-octanol it partitions between the oil-excess or sub-phase (e.g. in oil-swollen micelles) and the amphiphilic film. Thus, on the one hand, the alcohol acts as a co-solvent making the oil more hydrophilic. On the other hand, the alcohol mixes into the amphiphilic film making it increasingly hydrophobic. Although the mean curvature H of the amphiphilic film is lowered by both effects, the latter is predominant since the OH-group of the alcohol is small compared to the large head groups of the sugar surfactant. Increasing the concentration of 1-octanol further, the film is enriched in 1-octanol and decreases its curvature until it inverts to form a water-in-oil (w/o) microemulsion (see Fig. 1.18). Accordingly, the tuning parameter δ_i in quaternary temperature-insensitive *n*-alkylglycoside systems plays the same role as the temperature in the ternary water–oil–C_iE_j systems. That this is indeed the case can be shown by scaling the phase behaviour. The corresponding scaling parameters for the quaternary temperature-insensitive microemulsions are $\tilde{\gamma}_i(\phi = 0.50)$, the lower limit $\delta_{i,l}$ and the upper limit $\delta_{i,u}$ of the three-phase body [61].

1.2.4 Microemulsions with ionic surfactants

In the preceding sections, the phase behaviour of rather 'simple' ternary and quaternary non-ionic microemulsions have been discussed. However, the first microemulsion found by Schulman more than 50 years ago was made of water, benzene, hexanol and the ionic-surfactant potassium oleate [1, 3]. Winsor also used the ionic-surfactant sodium decylsulphate and the co-surfactant octanol to micro-emulsify water/sodium sulphate and petrol ether [2]. In the last 30 years, in-depth studies on ionic microemulsions have been carried out [7, 8, 65, 66]. It turned out that nearly all ionic surfactants which contain one single hydrocarbon chain are too hydrophilic to build up microemulsions. Such systems can only be driven through the phase inversion if an electrolyte and a co-surfactant is added to the mixture (see below and Fig. 1.11).

However, using double-chain ionic surfactants, e.g. sodium-bis-ethylhexylsulfosuccinate (AOT) [9, 67] and didodecyl dimethyl ammonium bromide (DDAB) [68], no co-surfactant is necessary to tune the mean curvature of the amphiphilic film from positive to negative. In the following the quaternary (pseudo-ternary) system H_2O/NaCl (A)–*n*-decane (B)–AOT (D) will be discussed to show the main features of ionic microemulsions. Subsequently, the knowledge gained for alkylpolyglucoside microemulsions (see Section 1.2.3) will be applied to understand the complex behaviour of five component ionic mixtures.

1.2.4.1 Quaternary AOT microemulsions

AOT has become the most widely studied amphiphile to formulate ionic microemulsions because only traces of an inert electrolyte shifts the phase inversion of the H_2O–oil–AOT system to ambient temperatures. In general, an ionic amphiphile gets more hydrophilic with increasing temperature which is in contrast to the non-ionic alkyl polyglycol ethers mentioned above (see Section 1.2.1). This increase in hydrophilicity can be attributed to the increasing effective degree of dissociation of the counterions at higher temperatures. The opposite effect is achieved by the addition of electrolytes to ionic microemulsions. The salt ions compete with the counterions and the head groups for water of hydration and decrease the hydrophilicity of the surfactant. This combination of adding salt and increasing the temperature can be used to tune the mean curvature of the amphiphilic film and with it the phase behaviour of the quaternary AOT microemulsion [67].

Considering the phase behaviour of the system H_2O/NaCl (A)–*n*-decane (B)–AOT (D) as an example, the temperature-dependent phase behaviour of the system can be represented as a first approximation in an upright Gibbs phase prism, if the mixture of H_2O and NaCl (often referred to as brine) is treated as a pseudo-component. It holds for the mass fraction of NaCl in the H_2O/NaCl mixture

$$\varepsilon = \frac{m_{\text{salt}}}{m_{\text{salt}} + m_{\text{water}}}. \tag{1.10}$$

As for the systems discussed above, the binary base systems are considered first to understand the phase behaviour of the pseudo-ternary ionic microemulsion. Brine (H_2O/NaCl) (A) and *n*-decane (B) are practically immiscible over the experimentally accessible temperature range. The binary system *n*-decane (B)–AOT (D) shows a lower miscibility gap that lies below the melting point of *n*-decane. Thus, a complete miscibility of *n*-decane and AOT exists between the melting and boiling points of *n*-decane. However, adding traces of water the situation changes and an upper miscibility gap appears [67]. As for the ternary non-ionic microemulsions the pseudo-binary system (H_2O/NaCl) (A)–AOT (D) plays the decisive role in the phase behaviour of the AOT microemulsion. As regards the binary system H_2O–AOT the lower miscibility gap with an upper critical point is covered by a lamellar phase that extends to low amphiphile concentrations. Adding NaCl one observes that the lamellar phase is pushed back, while simultaneously the miscibility gap is enlarged towards higher temperatures [69].

The phase behaviour of the pseudo-ternary ionic mixture can again be explained with the interplay of the three binary base systems. At low temperatures the ionic surfactant is

preferentially soluble in oil, at high temperatures in brine. Thus, having added the adequate amount of salt, an increase in temperature turns the ionic surfactant from hydrophobic at low into hydrophilic at high temperatures. On the microscopic level the temperature-dependent behaviour of ionic microemulions can be explained with changes of the mean curvature H of the amphiphilic film. Starting with a film which is curved around the water the degree of dissociation of the counterions increases, if the temperature is increased. This increasing degree of dissociation leads to stronger repulsive interactions between the ionic head groups on the water-side of the amphiphilic film. Accordingly, the mean curvature of the film inverts from being curved around the water ($H < 0$) to being curved around the oil ($H > 0$) as the temperature is increased.

In Fig. 1.10(a), the temperature dependence of the phase behaviour is shown by means of a $T(\gamma)$-section through the phase prism of the pseudo-ternary system H_2O/NaCl–*n*-decane–AOT at $\varepsilon = 0.006$ and an oil/(water + oil) mass fraction $\alpha = 0.50$. As can be seen, the phase boundaries of the ionic system also resemble the shape of a fish with a three-phase region at ambient temperatures. The three-phase region touches the one-phase region at $\tilde{T} = 29.0^{\circ}$C and $\tilde{\gamma} = 0.061$, which shows a rather good efficiency of the double-chain ionic surfactant AOT in solubilising brine and *n*-decane. At lower temperatures a water-in-oil (w/o) microemulsion coexists with a water excess phase ($\overline{2}$), whereas at higher temperatures an o/w microemulsions coexists with an oil excess phase ($\underline{2}$). Thus, a phase sequence of $\overline{2}$, 3, $\underline{2}$ is observed in the ionic system which is inverse to the $\underline{2}$, 3, $\overline{2}$ sequence found in non-ionic microemulsions. Despite this inverse temperature dependence the overall behaviour of both types of systems is rather similar. This analogy between the properties of pseudo-ternary ionic and ternary non-ionic microemulsions is another indication that the behaviour of microemulsions obviously follows a general pattern irrespective of the components they are made of.

The variation of the phase behaviour as a function of the salinity is shown in Fig. 1.10(b) in the form of an $\varepsilon(\gamma)$-section through the phase tetrahedron of the quaternary H_2O/NaCl–*n*-decane–AOT system at $\alpha = 0.50$ and a constant temperature of $T = 40^{\circ}$C. In order to compare the variation of the phase behaviour with temperature and salinity a rectangular representation is used also for the $\varepsilon(\gamma)$-section through the phase tetrahedron. As can be seen, the phase boundaries also resemble the shape of a fish in this isothermal $\varepsilon(\gamma)$-section. However, with increasing mass ε fraction of salt the phase sequence $\underline{2}$, 3, $\overline{2}$ is found which is inverse to the $\overline{2}$, 3, $\underline{2}$ sequence observed with increasing temperature.

The dependence of the phase behaviour on the salinity can also be explained by the interplay of the three binary base systems. At a constant temperature (e.g. $T = 40^{\circ}$C) and an amount of salt $\varepsilon = 0.006$ the ionic surfactant is preferentially soluble in brine ($\underline{2}$, see also Fig. 1.10(a)). Increasing ε makes AOT less hydrophilic, i.e. will enlarge the brine (A)–AOT (D) miscibility gap towards higher temperatures so that the AOT molecules become preferentially soluble in oil ($\overline{2}$). The mean curvature of the amphiphilic film is curved around the oil at low ε. As the addition of salt leads to an increasing screening of the electrostatic interactions between the ionic head groups on the water-side of the amphiphilic film, the mean curvature of the film inverts from being curved around the oil ($H > 0$) to being curved around the water ($H < 0$) with increasing ε. Thus, the tuning parameter salinity (ε) in quaternary ionic microemulsions plays the same role as the temperature in ternary systems water–oil–C_iE_j.

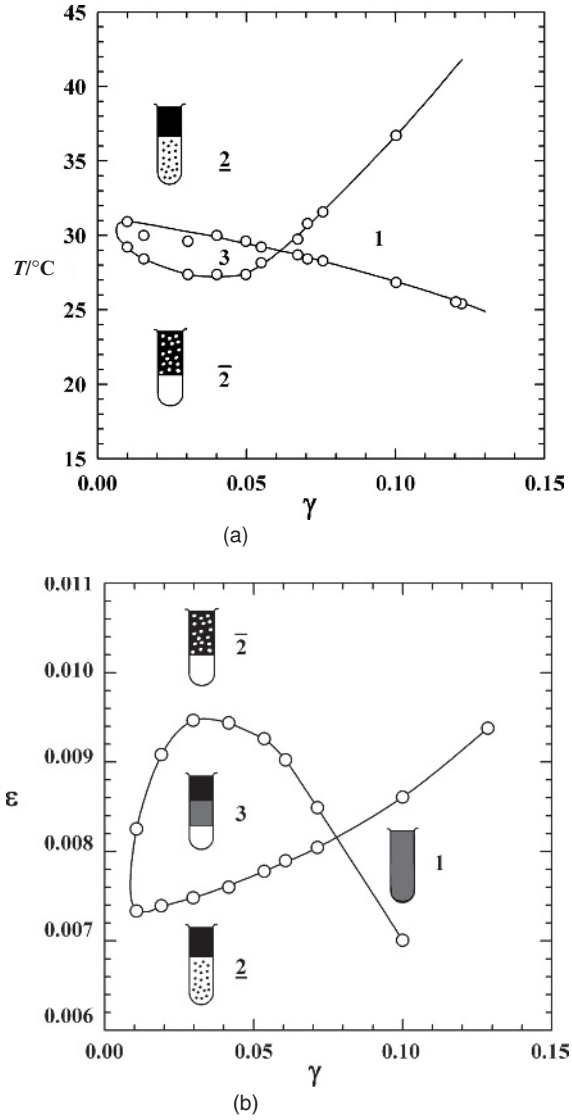

Figure 1.10 Phase behaviour of the ionic system H_2O/NaCl–*n*-decane–sodium-bis-ethylhexylsulfosuccinate (AOT) at a constant oil/(water + oil) mass fraction of $\alpha = 0.50$ [67]. (a) $T(\gamma)$-section performed at a constant salt mass fraction in water of $\varepsilon = 0.006$. The phase boundaries resemble the shape of a fish (general pattern of microemulsions!). Note that regarding the temperature dependence the phase sequence is inverted compared to that of non-ionic microemulsions. (b) $\varepsilon(\gamma)$-section through the phase tetrahedron of the quaternary system H_2O–NaCl–*n*-decane–sodium-bis-ethylhexylsulfosuccinate (AOT) at a temperature of $T = 40°C$. In this isothermal section the phase boundaries again resemble the shape of a fish. However, with increasing mass fraction of salt ε the phase sequence $\underline{2}$, 3, $\overline{2}$ is found due to the increasing screening of the electrostatic interactions.

1.2.4.2 Quinary SDS microemulsions

Ionic surfactants with only one alkyl chain are generally extremely hydrophilic so that strongly curved and thus almost empty micelles are formed in ternary water–oil–ionic surfactant mixtures. The addition of an electrolyte to these mixtures results in a decrease of the mean curvature of the amphiphilic film. However, this electrolyte addition does not suffice to drive the system through the phase inversion. Thus, a rather hydrophobic co-surfactant has to be added to invert the structure from oil-in-water to water-in-oil [7, 66]. In order to study these complex quinary mixtures of water/electrolyte (brine)–oil–ionic surfactant–non-ionic co-surfactant, brine is considered as one component. As was the case for the quaternary sugar surfactant microemulsions (see Fig. 1.9(a)) the phase behaviour of the pseudo-quaternary ionic system can now be represented in a phase tetrahedron if one keeps temperature and pressure constant.

As an example, the phase behaviour of the system H_2O/NaCl–*n*-decane–sodium dodecyl sulphate (SDS)–1-butanol (C_4E_0) will be discussed at a rather large salinity of $\varepsilon = 0.10$ and $T = 20°C$. Again, the systems representing the faces of the phase tetrahedron are considered first in order to understand the complex behaviour of the pseudo-quaternary system. Of major interest are the two-side systems H_2O/NaCl–*n*-decane–SDS and H_2O/NaCl–*n*-decane–C_4E_0. Both systems show miscibility gaps. Within the former system the SDS molecules prefer the water phase, i.e. a $\underline{2}$ miscibility gap is formed. In contrast, the latter system shows a $\overline{2}$ behaviour, i.e. the C_4E_0 molecules reside mainly in the oil phase. Since there is an additional demixing tendency in the third ternary-side system H_2O/NaCl–C_4E_0–SDS the formation of a three-phase region is induced inside the phase tetrahedron.

Equivalently to the quaternary sugar surfactant microemulsions the $w_D(w_C)$-sections through the tetrahedron are obtained experimentally by titrating a sample containing the desired amounts of brine, *n*-decane and SDS with the co-surfactant C_4E_0. Figure 1.11 shows such a section at $\phi = 0.58$, $\varepsilon = 0.10$ and $T = 20°C$. As can be seen, the phase boundaries obtained resemble the shape of the fish. At low mass fractions of SDS, the phase sequence $\underline{2}$, 3, $\overline{2}$ is found with increasing 1-butanol content. At higher mass fractions of SDS, the $\underline{2}$, 1, $\overline{2}$ sequence is observed. For even higher mass fractions a lamellar phase appears.

From Fig. 1.11 it is obvious that the phase behaviour of pseudo-quaternary ionic microemulsions follows the general patterns of microemulsions, which is mainly determined by the variation of the mean curvature H of the amphiphilic film. Starting from the pseudo-ternary system without 1-butanol, a small amount of the oil is already solubilised in the SDS-micelles due to the screening of the repulsive interaction between the ionic head group obtained by the addition of NaCl. Thus, an oil-in-water (o/w) microemulsion forms that coexists with an excess-oil phase ($\underline{2}$). Adding 1-butanol it partitions between the bulk oil phase and the bulk water phase as well as the amphiphilic film. Enriching the film with 1-butanol lowers H until the curvature inverts, i.e. a water-in-oil (w/o) microemulsion forms that coexists with an excess-water phase ($\overline{2}$). However, having driven the system through phase inversion (from $\underline{2}$ to $\overline{2}$) by adding 1-butanol the system can be tuned back to $\underline{2}$ by keeping the fraction δ_i of 1-butanol in the amphiphilic film constant and increasing the temperature.

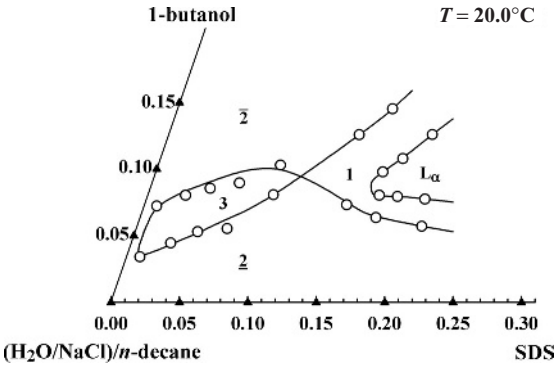

Figure 1.11 Section through the phase tetrahedron of the pseudo-quaternary system H_2O/NaCl–*n*-decane–sodium dodecyl sulphate (SDS)–1-butanol (C_4E_0) at $\phi = 0.58$, $\varepsilon = 0.10$ and $T = 20°C$ [26]. Note that the pseudo-quaternary ionic system can be driven through phase inversion by adding C_4E_0 as was the case for the quaternary alkylpolyglucoside microemulsions. (From Ref. [26], reprinted with permission of Elsevier.)

1.2.5 Microemulsions with non-ionic and ionic surfactants

In the previous section a quinary ionic microemulsion was tuned through the phase inversion by adding a short-chain alcohol as a non-ionic co-surfactant to a single-tailed ionic surfactant. In the following the short-chain alcohol is replaced by an ordinary long-chain non-ionic surfactant. It was discussed above that the temperature dependence of the phase behaviour of ionic (see Section 1.2.4) and non-ionic microemulsions (see Section 1.2.1) is inverse. Thus, one can expect that at a certain ratio δ of non-ionic and ionic surfactants the inverse temperature trends compensate so that a temperature-insensitive microemulsion forms. It goes without saying that this property is extremely relevant in technical applications, where often mixtures of non-ionic and ionic surfactants are used.

In order to locate the composition where most of the properties of the complex quinary (pseudo-quaternary) mixture are expected to be temperature-insensitive, time-consuming studies of the phase behaviour have to be performed. Such studies were carried out with the quinary system H_2O–NaCl–*n*-decane–$C_{12}E_4$–AOT [10]. The result is shown in Fig. 1.12 in the form of a $T(\gamma)$-section through the phase prism at $\phi = 0.60$ and $\varepsilon = 0.006$ considering H_2O/NaCl and $C_{12}E_4$/AOT, respectively, as a pseudo one-component system. In this study, a mass fraction of $\delta = 0.60$ of AOT in the $C_{12}E_4$/AOT mixture was chosen to obtain an almost temperature-insensitive phase behaviour. Note that only the phase boundaries of the one-phase region are determined experimentally, whereas the extension of the three-phase region is shown schematically. As can be seen, the phase boundaries around the $\tilde{X}$-point are very steep, which indicates the temperature insensitivity. Thus, preparing a mixture of H_2O/NaCl–*n*-decane–$C_{12}E_4$–AOT at $\phi = 0.60$, $\delta = 0.60$, $\varepsilon = 0.006$ and an overall surfactant mass fraction of $\gamma = 0.08$ a one-phase microemulsion is obtained between 0 and 75°C.

In conclusion, the extensive study of the phase behaviour of different microemulsions provides detailed knowledge about the phase behaviour of microemulsions. As discussed above, it is emphasised that microemulsions show striking similarities in the phase

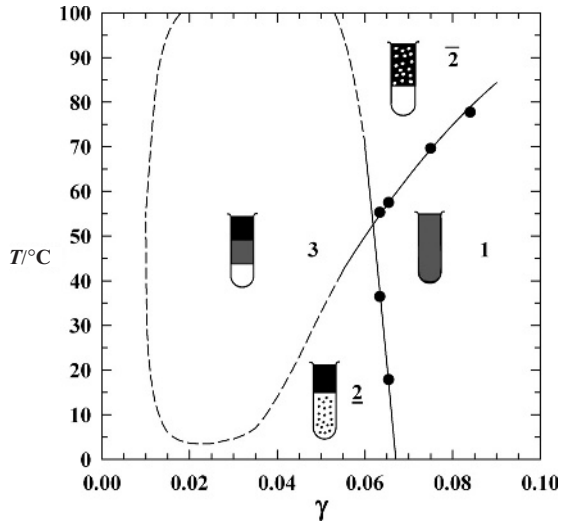

Figure 1.12 $T(\gamma)$-section of the quinary system H_2O/NaCl–*n*-decane–$C_{12}E_4$/AOT at constant $\phi = 0.60$, a mass fraction of $\delta = 0.60$ of AOT in the $C_{12}E_4$/AOT mixture and a salt mass fraction in water of $\varepsilon = 0.006$. Note that the steepness of the phase boundaries indicates their temperature-insensitivity. Furthermore, the $C_{12}E_4$/AOT mixture provides an efficient solubilisation ($\tilde{\gamma} = 0.06$) of the oil *n*-decane in water and vice versa. (From Ref. [26], reprinted with permission of Elsevier.)

behaviour irrespective of whether they are stabilised by pure non-ionic surfactants, technical-grade non-ionic surfactants, *n*-alkylpolyglucosides, ionic surfactants, or by mixtures of non-ionic and ionic surfactants. It turned out that several tuning parameters can be chosen to drive the system through the phase inversion, i.e. to obtain a zero-mean curvature of the amphiphilic film. These parameters can be the temperature T, the salinity ε, or the ratio δ_i of two different surfactants in the amphiphilic film.

1.3 Interfacial tension

Perhaps the most striking property of a microemulsion in equilibrium with an excess phase is the very low interfacial tension between the macroscopic phases. In the case where the microemulsion coexists simultaneously with a water-rich and an oil-rich excess phase, the interfacial tension between the latter two phases becomes ultra-low [70, 71]. This striking phenomenon is related to the formation and properties of the amphiphilic film within the microemulsion. Within this internal amphiphilic film the surfactant molecules optimise the area occupied until lateral interaction and screening of the direct water–oil contact is minimised [2, 42, 72]. Needless to say that low interfacial tensions play a major role in the use of microemulsions in technical applications [73] as, e.g. in enhanced oil recovery (see Section 10.2 in Chapter 10) and washing processes (see Section 10.3 in Chapter 10). Suitable methods to measure interfacial tensions as low as 10^{-3} mN m^{-1} are the sessile or pendent drop technique [74]. Ultra-low interfacial tensions (as low as 10^{-5} mN m^{-1}) can be determined with the surface light scattering [75] and the spinning drop technique [76].

As the latter is comparatively simple to use it can be regarded as the most suitable method to measure low and ultra-low interfacial tensions. In the following the general features of interfacial tensions in microemulsion systems are presented. The dramatic decrease of the water/oil interfacial tension upon the addition of surfactant, the correlation of interfacial tension and phase behaviour, the variation of the water/oil interfacial tension with the respective tuning parameter and the scaling of the interfacial tension will be discussed in detail. All data presented have been determined using the spinning drop technique [17].

1.3.1 Adsorption of the surfactant

The starting point of this discussion is the pure water–oil system. In the absence of surfactant the interfacial tension σ_{ab} of the water/oil interface is generally 30–50 mN m^{-1}. Adding small amounts of surfactant the molecules will either adsorb at the water/oil interface or be monomerically distributed between the water- (a) and oil-rich (b) phase. For ionic surfactants such as AOT the monomer is mainly soluble in the water phase ($\gamma_{Cmon,a} >> \gamma_{Cmon,b}$), while for non-ionics such as $C_{12}E_5$ the monomer is mainly soluble in the oil phase ($\gamma_{Cmon,a} << \gamma_{Cmon,b}$, see Section 1.2.1). The adsorption of the surfactants at the macroscopic water/oil interface and the increase of the monomer concentrations causes the interfacial tension σ_{ab} to drop to a value which may vary from a few mN m^{-1} to ultra-low values of 10^{-3}–10^{-4} mN m^{-1} [70]. A further addition of surfactant leads to a complete saturation of the water-rich and oil-rich phases as well as the water/oil interface with surfactant molecules so that the unfavourable water/oil contact is nearly perfectly screened. Above this concentration the excess surfactant molecules form aggregates in either the water, oil or a third phase (between the lower and upper limit of the three-phase body). Thus, the monomeric concentration of the surfactant in the water- and oil-rich phases as well as the water/oil interfacial tension stays practically constant.

Figure 1.13 shows the variation of the water/oil interfacial tension σ_{ab} as a function of the surfactant mass fraction γ (on a logarithmic scale) for a microemulsion at the mean temperature $\tilde{T}$ (i.e. PIT) of the three-phase body and equal volumes of water (A) and oil (B), i.e. $\phi = 0.5$, schematically [26]. As can be seen, σ_{ab} decreases from ~50 mN m^{-1} to almost zero if γ is increased (drawn line). At surfactant mass fractions above γ_0 a lens of a third phase, which is the microemulsion (c), is formed. The three test tubes illustrate the situation without surfactant (left), with only partially screened water/oil contact (centre) and at $\gamma > \gamma_0$ (right). Thus, as in aqueous surfactant solutions, the distinct discontinuity in the slope of the $\sigma_{ab}(\log\gamma)$-curve is an indication of the onset of aggregation. Below γ_0 the slope $(\delta\sigma_{ab}/\delta\log\gamma)$ is proportional to the interfacial concentration Γ_C of the surfactant which is given by the appropriate Gibbs equation [77]

$$\Gamma_C = -\frac{1}{2.303\,RT}\left.\frac{\partial\sigma_{ab}}{\partial\log\gamma}\right|_{T,p} \tag{1.11}$$

with R = gas constant. As is indicated by the dashed line in Fig. 1.13, the slope of the curve becomes practically constant already at concentrations well below γ_0 for most surfactant systems, whereas σ_{ab} continues to decrease rather steeply. This behaviour could

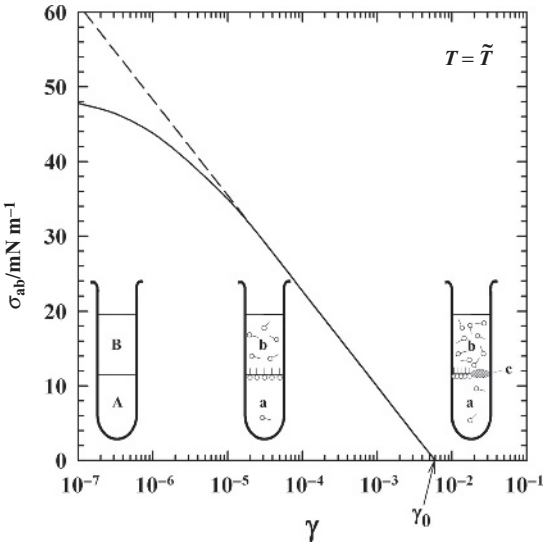

Figure 1.13 Schematic representation of the water/oil interfacial tension σ_{ab} (drawn line) as function of the non-ionic surfactant mass fraction γ at the mean temperature $\tilde{T}$ of the three-phase body. Starting from equal volumes of water (A) and oil (B), i.e. $\phi = 0.50$, the interfacial tension σ_{ab} decreases from 50 mN m^{-1} to values as low as 10^{-4} mN m^{-1}. After having crossed the monomeric solubility γ_0 of the surfactant in the water- and oil-rich phase, σ_{ab} remains constant. The test tubes illustrate the situation without surfactant (left), with only partially screened water/oil contact (centre) and at $\gamma > \gamma_0$, where the microemulsion phase (c) exist in form of a lens (right). (From Ref. [26], reprinted with permission of Elsevier.)

be interpreted as a consequence of the strong adsorption of the surfactants at the interface which saturates the water/oil interface well below γ_0. However, this would still raise the question why hardly measurable changes of Γ_C lead to a strong decrease of σ_{ab}. Knowing the interfacial concentration Γ_C in a saturated water/oil monolayer, the area per molecule $a_C = (N_A \Gamma_C)^{-1}$ can be determined [78, 79]. Another method to obtain reliable values of a_C in the water/oil interface is the analysis of experimentally more demanding SANS measurements [80] (see Chapter 2).

1.3.2 Interfacial tension and phase behaviour

From the above, it is clear that a pre-requisite of low water/oil interfacial tensions is the complete saturation of the water-rich and oil-rich phases as well as the water/oil interface by surfactant molecules. Of course, this pre-requisite is fulfilled if one of the phases considered is a microemulsion. Furthermore, since the pioneering work of Lang and Widom [81] it is known that if a system is driven through phase inversion the interfacial tensions may become ultra-low. However, about 20 years ago, a number of experimental investigations were devoted to clarifying the origin of the ultra-low interfacial tensions [15, 17, 39, 71, 81–85]. In order to understand this correlation between phase behaviour and interfacial

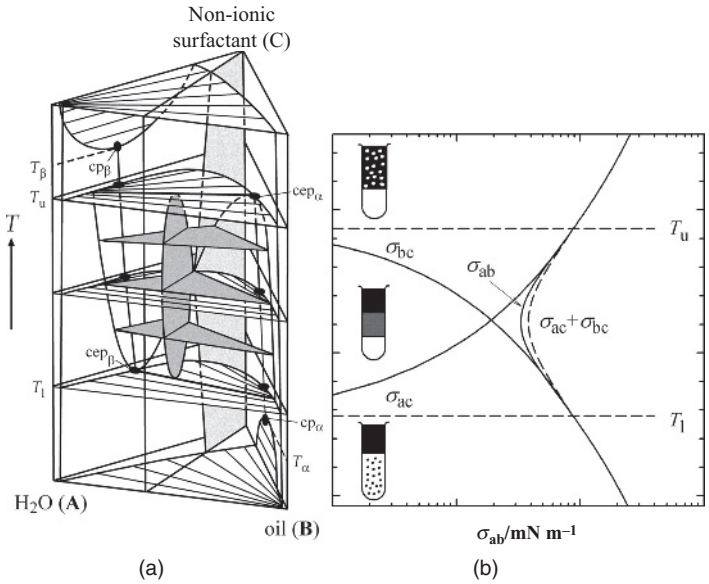

Figure 1.14 Schematic phase prism (a) and interfacial tensions (b) as function of temperature for the system water–oil–non-ionic surfactant. The minimum of the water/oil interfacial tension $\tilde{\sigma}_{ab}$ at $\tilde{T}$ is a consequence of the phase behaviour. Increasing the temperature the aqueous phases separates into the phases (a) and (c) at the critical endpoints cep_β whereas the phases (b) and (c) merge into a single oil-rich phase at cep_α. Thus, the interfacial tensions σ_{ac} and σ_{bc} show an opposite temperature dependence, becoming zero at T_l and T_u, respectively. Note that the interfacial tensions are plotted on a log-scale.

tensions, let us consider as an example the temperature dependence of both properties in ternary non-ionic microemulsion systems.

Figure 1.14(a) shows the phase prism of the system water–oil–non-ionic surfactant (already shown in Fig. 1.3) together with the temperature dependence of the interfacial tensions (Fig. 1.14(b)). As discussed in Section 1.2.1, at low temperatures, non-ionic surfactants mainly dissolve in the aqueous phase and form an oil-in-water (o/w) microemulsion (a) that coexists with an oil-excess phase (b). Thus, for temperatures below the temperature T_l the interfacial tension σ_{ab} refers to the interface between an o/w-microemulsion and an oil-rich excess phase. As the temperature is increased, the o/w-microemulsion separates into two phases (a) and (c) at the temperature T_l which, in turn, leads to the appearance of the three-phase body. Thus, three different interfacial tensions occur within the three-phase body, namely the interfacial tension between the water-rich and the surfactant-rich phase σ_{ac}, between the oil-rich and the surfactant-rich phase σ_{bc}, and between the water-rich and the oil-rich phase σ_{ab}. However, the latter can only be measured if most of the surfactant-rich middle phase (c) is removed, which then floats as a lens at the water/oil interface. Increasing the temperature one observes that the three-phase body vanishes at the temperature T_u, where a water-in-oil (w/o) microemulsion is formed by the combination of the two phases (c) and (b). Therefore, at temperatures above T_u the interfacial tension σ_{ab} refers to the interface between a w/o-microemulsion and a water-rich excess phase.

From the temperature dependence of the phase behaviour the qualitative shape of the three interfacial tension curves can be deduced. As the two phases (a) and (c) are identical at the critical tie line at T_l the interfacial tension σ_{ac} has to start from zero and increases monotonically with increasing temperature. Whereas the interfacial tension σ_{bc} decreases (monotonically) with increasing temperature and vanishes at T_u, because the two phases (c) and (b) become identical at the critical tie line at T_u. This opposite temperature dependence of σ_{ac} and σ_{bc} results in a minimum if one considers the sum of the two, $\sigma_{ac} + \sigma_{bc}$. In order to assure the stability of the water/oil interface

$$\sigma_{ab} \leq \sigma_{ac} + \sigma_{bc} \tag{1.12}$$

must hold [83]. Otherwise a thin layer of the middle phase would form between the water- and oil-rich excess phase, which is the case for well-structured microemulsions (see Section 1.2.1, Fig. 1.7 and Section 1.4) only near the critical endpoints [41, 86]. Consequently, also σ_{ab} has to pass through a minimum at the mean temperature of the three-phase body $T_m = (T_u + T_l)/2$, i.e. at the PIT. Thus, the minimum of the water/oil interfacial tension $\overline{\sigma}_{ab}$ can be found at the same temperature where the solubilisation of water and oil is obtained with the minimum amount of surfactant $\tilde{\gamma}$.

Furthermore, knowing σ_{ab}, T_l and T_u, the relative location of the individual σ_{ac}- and σ_{bc}-curves is fixed. Near the critical endpoint temperatures T_l and T_u even a quantitative description of the interfacial tensions σ_{ac} and σ_{bc} can be obtained applying the scaling laws

$$\sigma_{ac} = \sigma_{ac,0}\varepsilon^{\mu} \quad \text{and} \quad \sigma_{bc} = \sigma_{bc,0}\varepsilon^{\mu}, \tag{1.13}$$

where $\mu = 1.26$ is the critical exponent [82, 83, 85], $\sigma_{ac,0}$, $\sigma_{bc,0}$ are the critical amplitudes and $\varepsilon = |T_i - T|/T_i$ is the distance from T_l and T_u, respectively.

1.3.3 Tuning parameters for the interfacial tension σ_{ab}

As was mentioned earlier, it is above all the water/oil interfacial σ_{ab} that plays an important role in technical applications. Thus, much work has been carried out to obtain the variation of σ_{ab} as a function of the respective tuning parameter, i.e. temperature T [17, 84, 87, 88], salinity ε[15, 89] and co-surfactant to surfactant ratio δ[16, 90]. In the following the variation of the water/oil interfacial as a function of temperature and composition of the amphiphilic film (see Section 1.2.3) is discussed by way of example.

Figure 1.15(a) shows the variation of the interfacial tension σ_{ab} with the temperature for the system water–*n*-octane–$C_{10}E_4$ [17] and σ_{ab} as a function of the composition of the amphiphilic film $\delta_{V,i}$ ($\delta_{V,i}$ is the volume fraction and can be calculated by replacing m in Eq. (1.9) with V) in the quaternary system H_2O–*n*-octane–β-C_8G_1–C_8E_0 at $T = 25°C$ (Fig. 1.15(b)) [90]. In both cases a log-scale is used for the interfacial tension because of the strong variation over several orders of magnitudes.

As can be seen independently of the parameter used to drive the system through the phase inversion the shape of the interfacial tension curves is similar. Because of the fundamental link of the interfacial tension and phase behaviour discussed above, both systems show

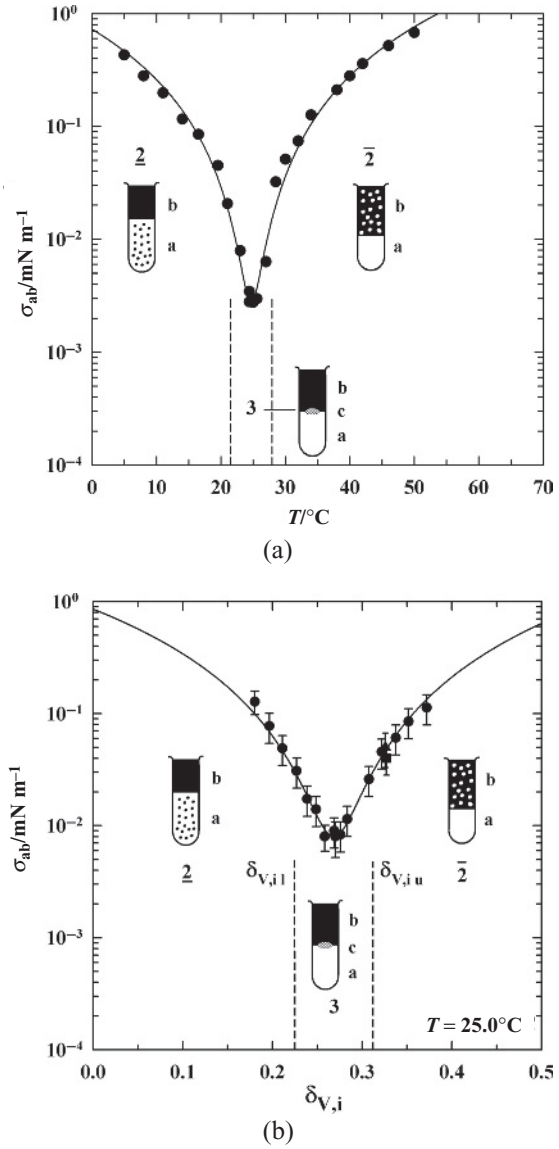

Figure 1.15 Water/oil interfacial tension σ_{ab} (plotted on log-scale) as function of the relevant tuning parameter. (a) Variation of σ_{ab} with temperature T, exemplarily shown for the water–*n*-octane–$C_{10}E_4$ system [17]. (b) Variation of σ_{ab} with the composition of the amphiphilic film $\delta_{V,i}$ in the quaternary system H_2O–*n*-octane–β-C_8G_1–C_8E_0 at $T = 25°C$ [90]. Both systems show that the water/oil interfacial tension runs through a distinct minimum in the middle of the three-phase region. The full line is calculated considering the bending energy difference between a curved amphiphilic film in the microemulsion and the flat film of the macroscopic interface [96].

an extreme minimum of the interfacial tension $\overline{\sigma}_{ab}$ in the three-phase region around $T_m = (T_u + T_l)/2$ and $\delta_{V,i,m} = (\delta_{V,i,l} + \delta_{V,i,u})/2$, respectively. The minimum of the water/oil interfacial tension is found to be ultra-low, i.e. $\overline{\sigma}_{ab} = 0.003$ mN m^{-1} in the $C_{10}E_4$ system and $\overline{\sigma}_{ab} = 0.008$ mN m^{-1} in the β-C_8G_1 system. Increasing the distance from the three-phase body the interfacial tension between the microemulsion and an excess-phase ($\underline{2}$- or $\overline{2}$-state) increases up to $\sigma_{ab} \approx 1$ mN m^{-1}.

A quantitative description of the variation of the water/oil interfacial tension with the respective tuning parameter can be obtained via the bending energy difference between a curved amphiphilic film in the microemulsion and the flat film of the macroscopic interface [25, 91]. The bending energy approach is based on Helfrich's mechanical model which describes vesicles by an ensemble of fluctuating amphiphilic films [92]. Later this membrane model was used to describe the properties of microemulsions [93–95]. The parameters which characterise the properties of the amphiphilic film are the bending rigidity κ, the saddle splay modulus $\overline{\kappa}$ and the spontaneous curvature of the film H_0 (see also Section 1.4 and Chapter 2). Interestingly, the drawn lines in Fig. 1.15, calculated from the analysis of the interfacial tension measurement in terms of bending energy, describe the data points quantitatively within the experimental error. Thus, the analysis of the macroscopic interfacial tension measurements is one of the few methods to determine the microscopic parameters κ and $\overline{\kappa}$ [17, 25, 91]. For more details the reader is referred to the quoted literature.

In Fig. 1.16, the variation of the water/oil interfacial tension with temperature is shown for four representative systems, namely water–*n*-octane–C_6E_2, C_8E_3, $C_{10}E_4$ and $C_{12}E_5$. In

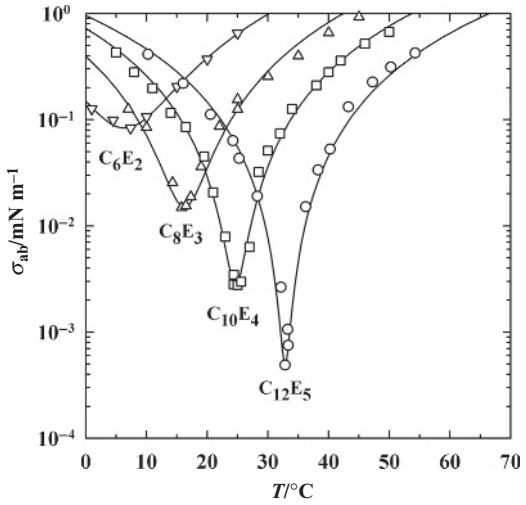

Figure 1.16 Temperature dependence of the water/oil interfacial tension σ_{ab} (plotted on log-scale) for some representative water–*n*-octane–C_iE_j systems. Note that the minimum of the interfacial tension curves $\overline{\sigma}_{ab}$ decreases substantially by increasing both the hydrophobic chain length *i* and the size of the hydrophilic head group *j* of the surfactants. The shift on the temperature scale stems from the shift of the phase behaviour. The full line is again calculated from an analysis of interfacial tensions in terms of the bending energy model [96]. (Figure redrawn with data from Ref. [17].)

this series the surfactant size is increased from C_6E_2 to $C_{12}E_5$ by increasing both i and j. As can be seen, the interfacial tension curves shift to higher temperatures, as do the three-phase bodies (see Fig. 1.4). Even more striking is the strong decrease of the minimum of the interfacial tensions $\overline{\sigma}_{ab}$ with increasing chain length of the surfactant shifting from system to system by one order of magnitude to lower values [17]. But, although the curves sharpen as the surfactant chain becomes longer, the shape remains similar. The full line which is calculated from the analysis of the interfacial tension experiment in terms of bending energy describes the data points again quantitatively within the experimental error. The value of the bending rigidity κ obtained from this analysis increases (as expected) with the surfactant chain length from values of about 0.6 kT to 1.1 kT [17].

1.3.4 Scaling of the interfacial tension σ_{ab}

The similar shape of the interfacial tension curves – which is obviously independent of the tuning parameter – suggests a scaling of the σ_{ab}-curves. The steepness of the interfacial tension curves around the centre of the three-phase body (i.e. around T_m or $\delta_{V,i,m}$) seems to correlate directly with the height of the three-phase body ($\Delta T = T_u - T_l$ or $\Delta\delta_{V,I} = \delta_{V,i,u} - \delta_{V,i,l}$). Thus, after centring the $\sigma_{ab}(T)$-curves by subtracting T_m or $\delta_{V,i,m}$ the axis of the respective tuning parameter can be normalised by $\Delta T/2$ or $\Delta\delta_{V,i}/2$, respectively. A reasonable normalisation of the interfacial tension axis is obtained using the minimum of the interfacial tension $\overline{\sigma}_{ab}$ [96]. Apart from this, however, one can follow Volmer's method [45, 46] to correlate $\overline{\sigma}_{ab}$ with the volume fraction of surfactant in the amphiphilic film of the optimum microemulsion, i.e. at the $\tilde{X}$-point at $\phi = 0.5$. Vollmer argued that colloidal dispersions should become thermodynamically stable if the interfacial free energy times the area of the colloidal object is provided by the thermal energy kT, i.e.

$$\sigma_{ab}\xi^2 \approx kT, \tag{1.14}$$

where ξ is the characteristic length scale of the colloidal object. Applied to microemulsions this relation holds for various types of structures [25, 87, 97] including the optimum microemulsion, which was found to have a bicontinuous structure [20, 21, 98, 99] (see also Fig. 1.20, Section 1.4). Since for bicontinuous microemulsions the characteristic length scale ξ is inversely proportional to the volume fraction $\phi_{C,i} + \phi_{D,i}$ of surfactant and co-surfactant (if present) in the amphiphilic film [42–44] (see also Section 1.4) one obtains for the minimum interfacial tension

$$\overline{\sigma}_{ab} \propto \left(\overline{\phi_{C,i} + \phi_{D,i}}\right)^2, \tag{1.15}$$

which has been confirmed experimentally [37, 71]. This finding suggests to normalise the interfacial tension by the squared volume fraction $\left(\overline{\phi_{C,i} + \phi_{D,i}}\right)^2$ of surfactant and co-surfactant (if present) in the amphiphilic film at the $\tilde{X}$-point at $\phi = 0.5$.

Figure 1.17 shows the scaling of interfacial tension curves for four ternary water–n-octane–C_iE_j systems (see Fig. 1.16) and the quaternary system water–n-octane–β-C_8G_1–C_8E_0 (see Fig. 1.15). As can be seen, the scaled $\sigma_{ab}(T)$-curves collapse onto one single curve, irrespective of the tuning parameter. However, some rather small, but systematic deviations

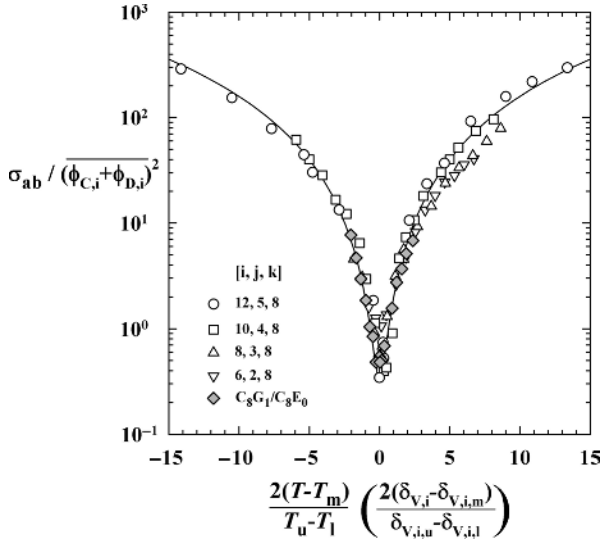

Figure 1.17 Scaling of the variation of the water/oil interfacial tension with the respective tuning parameter for four ternary water–*n*-octane–C_iE_j systems (see Fig. 1.16) and the quaternary system water–*n*-octane–β-C_8G_1–C_8E_0 (see Fig. 1.15). The tuning parameter T ($\delta_{V,i}$) is reduced by subtracting the mean temperature T_m (composition $\delta_{V,i,m}$) of the three phase body and normalising by $(T_u - T_l)/2$ $((\delta_{V,i,u} - \delta_{V,i,l})/2)$. Dividing σ_{ab} by the squared volume fraction $\left(\overline{\phi_{C,i} + \phi_{D,i}}\right)^2$ of surfactant and co-surfactant (if present) in the amphiphilic film of the optimum microemulsions ($\tilde{X}$-point at $\phi = 0.5$) the data of all systems lie on top of each other which emphasises the general patterns of microemulsions. The full line is again calculated from an analysis of interfacial tensions in terms of the bending energy model [96].

remain, above all in the three-phase region. These deviations were eliminated eventually by a more detailed analysis which has been used to calculate the full line in Fig. 1.17 [96]. To conclude this section it should be emphasised that the minimum in the water/oil interfacial tension at the centre of the three-phase body enables the optimal solubilisation of water and oil, i.e. with the minimum amount of surfactant $\tilde{\gamma}$. This correlation between phase behaviour and interfacial tension also holds for technical applications. For example, the removal of hexadecane from synthetic tissue reaches a maximum within the three-phase region (see Fig. 8.12 in Chapter 8) [100, 101]. Furthermore, the interfacial tension curves can be scaled with the same tuning parameters as the phase behaviour.

1.4 Microstructure

Most of the recent applications of microemulsions depend on the fact that microemulsions, though macroscopically homogeneous, are heterogeneous on the sub-microscopic scale. Topologically ordered interfacial films are formed by the surfactant molecules which are forced into the microscopic water/oil interface because of their amphiphilicity. The nature and properties of these microscopic interfacial films are essential for microemulsions as a whole and, in particular, for the most interesting feature of microemulsions, i.e. their microstructure. In the 1950s, Winsor [2] and Schulman [102] suggested that microemul-

sions are always spherical, and that a layered, lamellar structure exists as an exceptional phenomenon in the middle phase. In 1976, Scriven [98] put forward the crucial idea of the bicontinuous structure of the surfactant-rich middle phase, which 10 years later was proven with the help of NMR self-diffusion measurements [20, 21] and the direct visualisation by freeze-fracture electron microscopy (FFEM) [20, 22]. Further studies of the microstructure by NMR self-diffusion, TEM and scattering techniques (SAXS and SANS) revealed droplet-like and wormlike microemulsions, sample spanning networks and bicontinuous structures. Furthermore, liquid crystalline phases such as the cubic (V), hexagonal (H) and lamellar phases (L_α) exist and compete with these complex fluids. It has been realised that the main parameter determining the microstructure is the mean curvature of the amphiphilic interfacial film. Thus, controlling the curvature is the ultimate goal in order to be able to choose any desired structure.

1.4.1 Mean curvature of the amphiphilic film

The mean curvature of the amphiphilic film is given by

$$H = \frac{1}{2}(c_1 + c_2), \tag{1.16}$$

where $c_1 = 1/R_1$ and $c_2 = 1/R_2$ are the principal curvatures at a certain point on the film. By definition curvatures are positive if the amphiphilic film tends to enclose oil (o/w-microemulsions) and negative if it tends to enclose water (w/o-microemulsions). Parameters on which the curvature of the amphiphilic film depends are the temperature, the composition of the amphiphilic film, the salinity, etc. The mean curvature H, which can be determined experimentally by scattering techniques [25] (see Chapter 2), is closely related to the spontaneous curvature H_0, which is the curvature the interfacial film will adopt if no external forces, thermal fluctuations or conservation constraints exist. Both H_0 and the Gaussian curvature $K = c_1 c_2$ are important parameters in Helfrich's bending energy [92].

Figure 1.18 schematically shows the variation of the mean curvature H of the amphiphilic film for the temperature-sensitive ternary water–oil–C_iE_j systems (Fig. 1.18(a)) and the temperature-insensitive quaternary water–oil–C_nG_m–alcohol systems (Fig. 1.18(b)) by means of a wedge-shaped representation. As discussed above, for temperature-sensitive ternary systems one finds oil-in-water (o/w) microemulsions at low and water-in-oil (w/o) microemulsions at high temperatures due to a change of the mean curvature H of the amphiphilic film. At low temperatures the size of the surfactant head group is larger than that of the hydrophobic chain which curves the amphiphilic film around the oil. With increasing temperature, the size of the surfactant head group shrinks due to a dehydration, whereas the size of the hydrophobic chain increases due to an increasing number of chain conformations and the increasing penetration of oil molecules. Thus, H changes gradually from $H > 0$ to $H < 0$, i.e. from oil-in-water (o/w) to water-in-oil structures (w/o) structures via a locally planar amphiphilic film, i.e. $H = 0$ (Fig. 1.18(a)).

In Sections 1.2.3 and 1.3.3, it was shown that in temperature-insensitive quaternary C_nG_m systems the composition of the amphiphilic film instead of the temperature has to

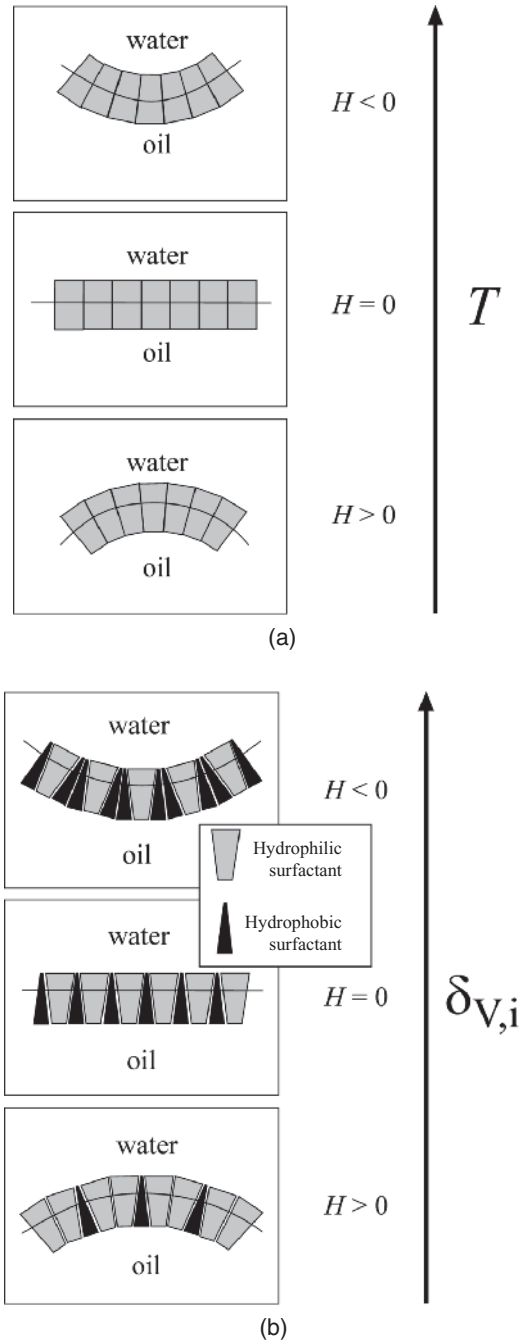

Figure 1.18 Mean curvature H of a non-ionic surfactant film at the water/oil interface as a function of temperature T (a) [26] and composition of the internal interface $\delta_{V,i}$ (b) [90]. The decrease in H with increasing T is mainly due to the shrinking size of the head group, while the decrease in H with increasing $\delta_{V,i}$ is due to the smaller head group area of the alcohol compared to the sugar surfactant. In order to illustrate this behaviour, a wedge-shaped representation has been chosen.

be varied to tune the phase behaviour and the interfacial tensions of the system. Recalling the results for these systems, we may conclude that the variation of the composition of the amphiphilic film changes its curvature. Figure 1.18(b) schematically shows this change of the curvature with increasing fraction of alcohol in the amphiphilic film. Knowing that the head group area of alcohols [80] is smaller than that of the sugar surfactants [103], one observes that an increasing fraction of alcohol in the mixed interfacial film causes a decrease of the mean curvature from $H > 0$ for o/w-microemulsions to $H < 0$ for w/o-microemulsions. In other words, the composition of the amphiphilic film is the tuning parameter of the mean curvature in quaternary temperature-insensitive systems.

Having understood the variation of the curvature of the amphiphilic film qualitatively the next step is to determine the variety and length scale of the microstructure and with it the underlying curvature of the amphiphilic film quantitatively. However, to gain a comprehensive insight into the structure pattern of microemulsions several different experimental methods have to be employed. Direct and local information about the occurring types of nano-structures can be provided by transmission electron microscopy [20, 99, 104, 105] (see Section 1.4.2). Statistical information about frequently occurring distances can be obtained from scattering techniques (see Chapter 2). Detailed information about the length scale of the microstructure can be gained from SAXS [106] and SANS [24]. Because of the relatively large wavelength, static light scattering (SLS) usually provides [107] only very unspecific information. What is somewhat more useful is dynamic light scattering (DLS) [108], which yields the diffusion coefficient of the structural domains. Furthermore, indirect methods like NMR self-diffusion [109] and electric conductivity [110] measurements provide valuable information on the connectivity of the microstructure and the transition from one type of structure to another. Each of the techniques provides a piece in the puzzle of the structure of microemulsions. In the following only results obtained by transmission electron microscopy will be discussed, while results obtained by scattering techniques are described in Chapter 2.

1.4.2 Transmission electron microscopy

In order to use electron microscopy to visualise the microemulsion structure, the problem of the fixation of the liquid mixtures has to be solved. The method of choice is to solidify the microemulsion structure via cryofixation. However, given that the phase behaviour as well as the curvature of the amphiphilic film (see Fig. 1.18) and with it the microstructure of most microemulsions show a strong temperature-dependence it has to be ensured that the cooling rate should be as high ($>10^4$ K/s) and the reorganisation kinetics of the microstructure as slow as possible.

Three different techniques, namely FFEM [20, 22], Cryo-Direct Imaging (Cryo-DI) [104] and freeze-fracture direct imaging (FFDI) [105], can be used to visualise the structure of microemulsions. In FFEM the samples are prepared in a protected fashion in a sandwich. They are then rapidly frozen, fractured, shadowed with metal, and replicated with a thin carbon film. The replica of the fractured surface, the morphology of which is controlled by the sample's microstructure, is then studied by a TEM. In contrast to FFEM, in Cryo-DI thin films of the sample are rapidly frozen but immediately, without replication, trans-

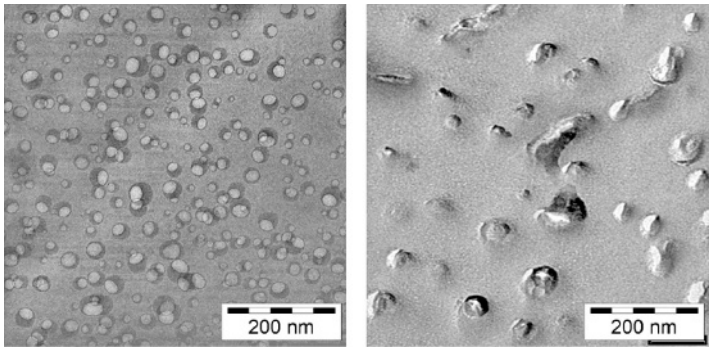

Figure 1.19 Micrographs of microemulsion droplets of the o/w-type in the system H_2O–*n*-octane–$C_{12}E_5$ prepared near the emulsification failure boundary at $\gamma_a = 0.022$, $w_B = 0.040$ and $T = 26.1°C$. (a) Freeze-fracture direct imaging (FFDI) picture showing dark spherical oil droplets of a mean diameter $<d> = 24 \pm 9$ nm in front of a grey aqueous background. Note that each oil droplet contains a bright domain of elliptic shape which is interpreted as voids. (b) The freeze-fracture electron microscopy (FFEM) picture supports the FFDI result. Each fracture across droplets which contain bubbles shows a rough fractured surface. (From Ref. [26], reprinted with permission of Elsevier.)

ferred to a low temperature stage within the microscope and imaged directly. In order to obtain these thin films (which have to be thin enough to allow for the electrons to transverse the sample) the sample has to be blotted prior to the vitrification. However, using this blotting technique a change of the concentration of the sample and a shearing of the internal microstructure are unavoidable. The recently developed FFDI method which is a hybrid of FFEM and Cryo-DI has solved the problems of the direct imaging technique. Like in FFEM, the sandwich method is used. However, after the sample is vitrified and fractured it is not shadowed and replicated but directly imaged. Thus, the FFDI technique avoids some experimental artifacts produced by the blotting of the sample using Cryo-DI. A disadvantage of the FFEM and FFDI techniques is the noticeably smaller cooling rate compared to the Cryo-DI-method, which can be attributed to the preparation and slower vitrification of the sample sandwich. Despite all sources of error which could be encountered during the sample preparation, reliable images of microemulsions can be obtained. In the following images of H_2O–*n*-octane–$C_{12}E_5$ microemulsions will be shown for which an o/w-, a w/o- and a bicontinuous microemulsion could have been visualised using both the FFEM and FFDI techniques.

Figure 1.19 shows micrographs [26, 111] of this ternary microemulsion prepared at low temperatures ($T < T_l$), where the amphiphilic film should be curved around the oil (see Fig. 1.18(a)), i.e. $H > 0$. To be more accurate the sample was prepared within the one-phase region near the emulsification failure boundary (see Fig. 1.7(b)) at the water-rich side ($\gamma_a = 0.022$, $w_B = 0.040$ and $T = 26.1°C$). Both the FFDI (Fig. 1.19(a)) and the FFEM picture (Fig. 1.19(b)) prove the existence of *n*-octane-swollen micelles in a water matrix. The FFDI picture shows dark spherical oil droplets of a mean diameter $<d> = 24 \pm 9$ nm in front of a bright aqueous background. Surprisingly, each oil droplet contains an elliptically shaped bright domain. These domains could be an artifact of the sample

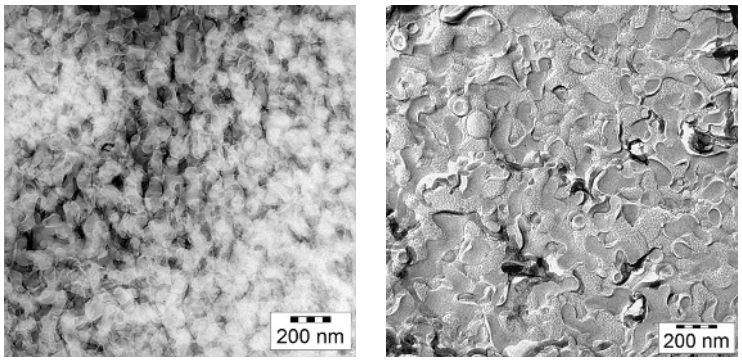

Figure 1.20 Micrographs of a bicontinuous microemulsion of the system H_2O–*n*-octane–$C_{12}E_5$ prepared near the $\tilde{X}$-point at $\phi = 0.50$, $\gamma = 0.06$ and $T = 32.4°C$. (a) Freeze-fracture direct imaging (FFDI) picture showing particularly in the middle of the image a sponge-like bicontinuous structure consisting of 'white' and 'black' domains. Note that the colours are inverted. (b) The freeze-fracture electron microscopy (FFEM) picture supports the FFDI result. (From Ref. [105], reprinted with permission of the American Chemical Society.)

preparation. Cooling the oil-in-water microemulsion rapidly from $T = 26.1°C$ to liquid nitrogen temperature $T = -196°C$, first the water is vitrified. Because of the different dependencies of the density of water and *n*-octane on temperature the still liquid *n*-octane droplets are now entrapped in a rigid matrix and contract. Thus, a differential stress is created that leads to the rupture of the fluid oil droplets and the resulting voids could be the elliptically shaped bright domains which can be seen in each *n*-octane droplet in the FFDI picture. The FFEM picture of the same sample shown in Fig. 1.19(b) supports the FFDI result. In fractures across the droplets one can see that the droplets in part exhibit planar fractures but in other places show a rough surface. Although the mean diameter of the oil-in-water droplets is difficult to determine from the FFEM picture it is obvious that their size is comparable to the FFDI result.

Micrographs of a bicontinuous microemulsion prepared near the $\tilde{X}$-point ($\phi = 0.50$, $\gamma = 0.06$, $T_m \approx \tilde{T} = 32.62°C$) are shown in Fig. 1.20. Again the FFDI (Fig. 1.20(a)) and the FFEM micrograph (Fig. 1.20(b)) are taken from the same sample [105]. Looking at the picture taken with the conventional FFEM technique (see also Ref. [112]), one can easily distinguish oil-rich and water-rich domains because of the texture of the oil domains, which stems from the shadowing of the fractured surface with tantalum (Ta) and tungsten (W) [22]. It is caused by the differing nucleation probabilities and surface mobilities on the various substrates and should not be mistaken for the real microstructure. As can be seen, the fracture through the water domains is in most cases planar, whereas for the oil domains the fracture follows the amphiphilic film. This difference leads to a three-dimensional impression of the oil-domains. Furthermore, one clearly sees water-rich and oil-rich domains which are mutually intertwined in a sponge-like fashion showing many saddle-shaped structures. Typically, the two principal curvatures appear to be almost equal but of opposite signs, i.e. $c_1 = -c_2$. As a consequence, the mean curvature H of the amphiphilic film can be around 0, while the Gaussian curvature K is negative. In other

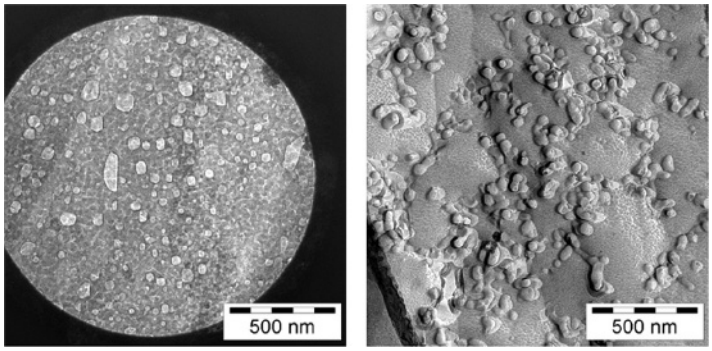

Figure 1.21 Micrographs of microemulsion droplets of the w/o-type in the system H_2O/NaCl–*n*-octane–$C_{12}E_5$ prepared near the emulsification failure boundary at a $\gamma_b = 0.050$, $w_B = 0.100$, $\varepsilon = 0.006$ and $T = 36.3°C$. (a) Freeze-fracture direct imaging (FFDI) picture showing bright water droplets of a mean diameter $<d> = 44 \pm 13$ nm against a dark oily background. (b) The freeze-fracture electron microscopy (FFEM) picture supports the FFDI result. The mean diameter of the water droplets is $<d> = 47 \pm 8$ nm. (From Ref. [105], reprinted with permission of the American Chemical Society.)

words, the structure is water-continuous and oil-continuous at the same time, a situation which is called *bicontinuous*. A similar situation is seen in the FFDI micrograph, i.e. in Fig. 1.20(a). Note that the colours are inverted to get images in which the details of the structure can be recognised more easily. In the middle of the image a sponge-like structure can be seen consisting of 'white' and 'black' domains. As this is a direct image through the sample, different numbers of layers of the structure are seen at each position. Comparing the length scale of the bicontinuous structures (i.e. the diameter ($d \approx 50$ nm) of the water and *n*-octane domains) visible in the FFEM and FFDI micrographs, one finds a good agreement between the two methods and the SANS [80] performed on a sample of similar composition.

Increasing the temperature and turning to the oil-rich side of the phase prism, one obtains micrographs of a water-in-oil microemulsion (see Fig. 1.21) [105]. The sample was prepared within the one-phase region near the water emulsification failure boundary (see Fig. 1.7(c)) of the ternary mixture H_2O/NaCl–*n*-octane–$C_{12}E_5$ at $\gamma_b = 0.050$, $w_A = 0.100$, $\varepsilon = 0.006$ and $T = 36.3°C$. The image obtained with the help of the conventional FFEM technique (Fig. 1.21(b)) shows water droplets in a continuous oil phase. As already mentioned, it is the decoration of the oil that allows distinction between the water- and oil-rich domains. Evaluating the FFEM image one obtains a mean diameter of the water droplets of $<d> = 47 \pm 8$ nm. Looking at the FFDI image (Fig. 1.21(a)), one clearly sees bright water droplets in the dark, textured *n*-octane matrix. For the size of the water droplets a mean diameter of $<d> = 44 \pm 13$ nm is found, which is in perfect agreement with FFEM and the SANS results [25]. Thus, comparing the FFEM and the FFDI image one clearly sees that the results are not only qualitatively but also quantitatively the same.

In conclusion, the transmission electron microscopy images show that for mixtures of water, oil and long-chain non-ionic surfactants the structure gradually changes with

increasing temperature from discrete oil-in-water micelles via a bicontinuous network to discrete water-in-oil micelles. Thus, as was already deduced from the variation of the phase behaviour, the mean curvature of the amphiphilic film changes from $H > 0$ at low temperatures to $H < 0$ at high temperatures. In between, at the PIT, $H = 0$ which is reflected in the bicontinuous structure. While a good deal of qualitative insight into the manifold structural properties is nicely gained, a more quantitative determination of parameters such as the length scale of the structure is difficult to infer from such images. As already mentioned above, detailed information about the length scale of the microstructure can be gained from scattering techniques, i.e. from SAXS and SANS, which are described in Chapter 2.

1.4.3 Estimation of length scales and overview of microstructure

Knowing the shape (topology) of the microstructure one can obtain an estimate of the length scales from the composition of the microemulsion. Thus, the diameter of the domains ($d = \xi$) in a bicontinuously structured microemulsion can be calculated from

$$\xi = a \frac{v_C}{a_C} \frac{\phi(1-\phi)}{\phi_{C,i}}, \tag{1.17}$$

where v_C and a_C are the volume and the area of the surfactant molecule, $\phi_{C,i}$ is the volume fraction of surfactant in the amphiphilic film, and a is a pre-factor, which depends on the model used to describe the bicontinuous structure. The model of Debye *et al.* [43] predicts $a = 4$, the Voronoi tessellation of Talmon and Prager [44] leads to $a = 5.84$ and the model of cubes by De Gennes and Taupin [42] yields $a = 6$. Experimentally, a somewhat larger factor of $a \approx 7$ is found from the analysis of SANS measurements [26, 80]. A rough estimation of the length scales of almost symmetric ($\phi = 0.5$) bicontinuous microemulsions can be obtained by

$$\xi \approx 1.5 \text{ nm}/\gamma. \tag{1.18}$$

To obtain Eq. (1.18) four things need to be assumed: (i) the monomeric solubility of the surfactant in water and oil can be neglected, (ii) $\delta = v_C/a_C \approx 1$ nm, (iii) $a = 6$ and (iv) the density of all components is the same. Furthermore, the radius of the spherical droplets can be calculated by

$$r_0 = 3 \frac{v_C}{a_C} \frac{\phi_i + \phi_{C,i}}{\phi_{C,i}} \frac{1+p^2}{1+3p^2}, \tag{1.19}$$

where ϕ_i denotes the volume fraction of the component solubilised in the respective micelles and p the polydispersity of an assumed Gaussian distribution of radii. Assuming again that $\delta = v_C/a_C \approx 1$ nm and that the density of all components is the same and neglecting the polydispersity and the monomeric solubility of the surfactant, one finds

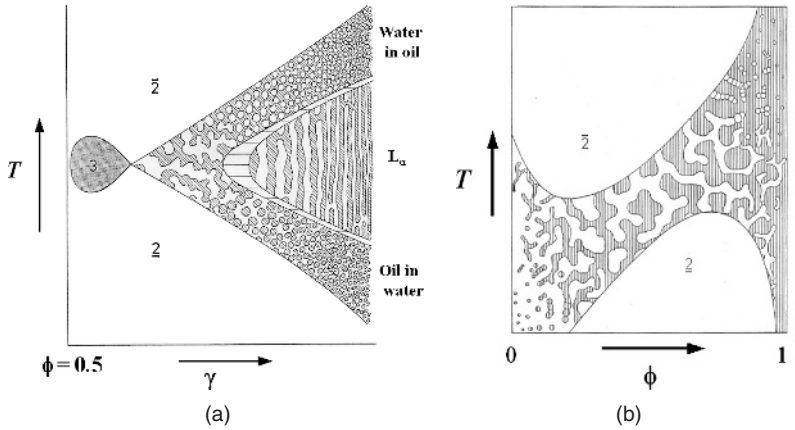

Figure 1.22 Schematic overview of the microstructure of non-ionic microemulsions as deduced from TEM, SANS, NMR-diffusiometry and electric conductivity together with the underlying phase behaviour. The shaded regions represent the oil and the white regions represent water. (a) $T(\gamma)$-section at $\phi = 0.5$ [25]. The variation of the curvature of the amphiphilic film with temperature becomes apparent by the change of microstructure from o/w- to w/o-droplet structures. Around $\tilde{T}$ bicontinuous structures can be found at low γ, whereas the lamellar phase L_α exists at higher γ. (b) $T(\phi)$-section through the phase prism at a constant $\gamma > \tilde{\gamma}$ (Shinoda cut) [114]. Within the homogeneous channel the microstructure changes from discrete o/w-structures on the water-rich side and low temperatures to discrete w/o-structures on the oil-rich side and high temperatures. (Figure redrawn with data from Ref. [17] and Ref. [18].)

that Eq. (1.19) simplifies to

$$r_0 = 3\frac{w_i + \gamma}{\gamma}\text{nm}, \tag{1.20}$$

with w_i being the weight fraction of the solubilised water or oil, respectively.

Studying the microstructure of microemulsions extensively by several different methods like TEM, SAXS, SANS, NMR diffusometry and electric conductivity, one can gain profound insights into their structure pattern. With respect to the ternary non-ionic microemulsion, the temperature dependence of the microstructure is presented in Fig. 1.22 in terms of two different sections through the prism. In Fig. 1.22(a), the microstructures existing within the extended one-phase region behind the $\tilde{X}$-point are drawn into the $T(\gamma)$-section (see Fig. 1.3) [25]. Starting at the $\tilde{X}$-point, i.e. close to the three-phase region, the structure of the microemulsion is bicontinuous with a zero-mean curvature of the amphiphilic film ($H = 0$), but a negative Gaussian curvature ($K < 0$). An increase of the surfactant mass fraction γ leads to a shrinking of the structure because the total area of the internal interface increases. At high surfactant concentrations the lamellar phase is observed, with a zero curvature structure, i.e. $H = 0$ and $K = 0$ ($c_1 = c_2 = 0$). Moving both γ- and temperature-wise away from the $\tilde{X}$-point one observes a transition to oil-in-water and water-in-oil droplets at low and high temperatures, respectively. Furthermore, the droplet size decreases as one moves further away from the $\tilde{X}$-point.

In order to study the variation of the microstructure as a function of the oil/(water + oil) volume fraction ϕ it has proved useful to perform a so-called Shinoda cut [113] ($T(\phi)$ section) through the phase prism at a constant mass fraction of surfactant $\gamma > \tilde{\gamma}(\phi = 0.50)$. Figure 1.22(b) shows a schematic drawing of this cut [114]. Within the one-phase channel on the water-rich side, the mixtures consist of stable dispersions of oil droplets in water that transform into a branched tubular oil network with rising temperature. Increasing ϕ, one finds sponge-like bicontinuous structures around the mean temperature of the three-phase body $T_m \approx \tilde{T}(\phi = 0.50)$, i.e. the PIT, if ϕ is varied between 0.2 and 0.8. On the oil-rich side, at high temperatures water droplets are found to be dispersed in a continuous oil-phase. These droplets transform into a branched tubular water network with decreasing temperature. Accordingly, the mean and Gaussian curvature of the amphiphilic film varies with temperature and composition. As mentioned before, other parameters to tune the curvature of the amphiphilic film are the salinity and the composition of the amphiphilic film, respectively.

1.5 Conclusion

The wide range of applications as well as the steadily increasing number of papers and patents on microemulsions already show their significance for many branches of chemistry and suggest that microemulsions will become even more significant in the future. The first chapter of this book dealt with the phase behaviour as well as the associated interfacial tensions and microstructures of microemulsions. The fact that these features are similar irrespective of what solvents and amphiphiles are used is a strong indication of the existence of a general microemulsion pattern. This general pattern is also mirrored in the fact that various tuning parameters lead to the same general observations.

We will conclude this chapter by summarising the most relevant properties of microemulsions. The system of choice is H_2O–*n*-octane–$C_{12}E_5$ as it has been studied very extensively [25]. Recalling the transmission electron microscopy images (see Fig. 1.20), one can observe a truly bicontinuous structure at the mean temperature of the three-phase body $T = T_m \approx \tilde{T}(\phi = 0.50)$. This result is supported by similar self-diffusion coefficients D of water and *n*-octane obtained from NMR self-diffusion measurements [115]. Figure 1.23 (top) shows the self-diffusion coefficients D plotted versus the temperature. As can be seen, the values of D for water and oil are nearly equal at the mean temperature (PIT) of the three-phase body, which is further evidence of the bicontinuity. Note that plotting the reduced self-diffusion coefficients D/D_0 (D_0 = self-diffusion coefficient of the pure solvents at the respective temperature) versus T indeed leads to equal D/D_0 values for both solvents at the PIT. At the PIT the length scale ξ of the structure shows a distinct maximum because of the optimal solubilisation of water and oil. Calculating the mean curvatures from the length scales by setting $H = 1/<r>$ and $H = -1/<r>$ for o/w- and w/o-microemulsions as well as $H = 0$ for the bicontinuous structure an almost linear decrease of the curvature is found with increasing temperature. As is seen in Fig. 1.23, H changes sign at $T = T_m$ [25, 26]. One further consequence of the length scale ξ reaching a maximum and the mean curvature changing its sign is that the interfacial tension σ_{ab} between the water and oil phases passes through a minimum at the PIT. Thus, knowing the variation of the curvature with the appropriate tuning parameter one cannot only adjust

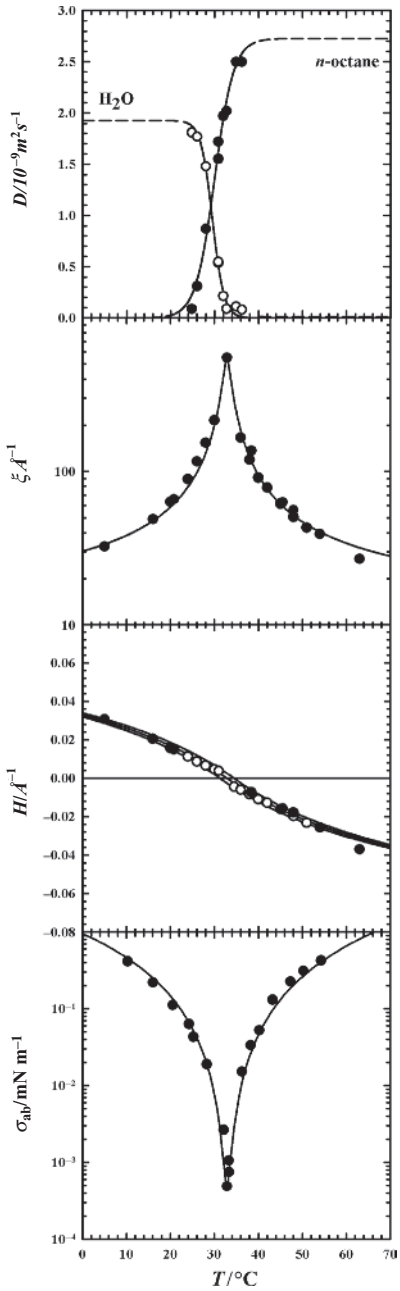

Figure 1.23 Variation of the water (shown as hollow symbols) and *n*-octane (shown as filled symbols) diffusion coefficients D_A and D_B [115], the length scale ξ [25], the mean curvature H and the water/oil interfacial tension σ_{ab} as function of the temperature for the system H_2O–*n*-octane–$C_{12}E_5$. Note that at the mean temperature of the three-phase body $\tilde{T}$ the diffusion of water and oil molecules is equal (points to bicontinuity), the length scale runs through a maximum, the curvature change sign and the water/oil interfacial shows an extreme minimum.

the desired shape and length scale of the structure but also the optimal solubilisation of water and oil via the ultra-low water–oil interfacial tension.

Acknowledgement

Thomas Sottmann wishes to thank Prof. Strey for his continuous financial and professional support. His thoughts and suggestions have been of great value. During the last 20 years of joint research and deep discussion a close friendship has evolved.

Notes

1. ISI Web of Knowledge, Science Citation Index Expanded.
2. European Patent Office, esp@cenet.

References

1. Schulman, J.H. and Hoar, T.P. (1943) Transparent water-in-oil dispersions: The oleopathic hydromicelle. *Nature*, **152**, 102.
2. Winsor, P.A. (1954) *Solvent Properties of Amphiphilic Compounds*. Butherworth & Co., London.
3. Schulman, J.H., Stoeckenius, W. and Prince, L.M. (1959) Mechanism of formation and structure of microemulsions by electron microscopy. *J. Phys. Chem.*, **63**, 1677–1680.
4. Sharma, M.K. and Shah, D.O. (1985) Macro- and microemulsions in enhanced oil recovery. In D.O. Shah (ed), *Macro- and Microemulsions Theory and Applications*, Vol. 272. American Chemical Society, Washington, DC, pp. 149.
5. Shinoda, K. (ed) (1967) *Solvent Properties of Surfactant Solutions*, Vol. 2. Marcel Dekker, New York, pp. 27–63.
6. Kahlweit, M. and Strey, R. (1985) Phase behavior of ternary systems of the type H_2O–oil–non-ionic amphiphile (microemulsions). *Angew. Chem. Int. Ed.*, **24**, 654–668.
7. Bellocq, A.M., Biais, J., Clin, B., Gelot, A., Lalanne, P. and Lemanceau, B. (1980) 3-Dimensional phase diagram of the brine–toluene–butanol–sodium dodecyl-sulfat. *J. Colloid Interface Sci.*, **74**, 311–321.
8. Langevin, D. (1986) Microemulsions and liquid crystals. *Mol. Cryst. Liq. Cryst.*, **138**, 259–305.
9. Eicke, H.F. (1982) The microemulsion concept in nonpolar surfactant solutions. In I.D. Robb (ed), *Mikroemulsions*. Plenum, New York, pp. 17–32.
10. Kahlweit, M. and Strey, R. (1988) Phase behavior of quinary mixtures of the type H_2O–oil–non-ionic amphiphile–ionic amphiphile–salt. *J. Phys. Chem.*, **92**, 1557–1563.
11. Kahlweit, M., Strey, R., Firman, P., Haase, D., Jen, J. and Schomäcker, R. (1988) General patterns of the phase behavior of mixtures of H_2O, nonpolar solvents, amphiphiles, and electrolytes. 1. *Langmuir*, **4**, 499.
12. Penders, M.H.G.M. and Strey, R. (1995) Phase behavior of the quaternary system H_2O/*n*-octane/C8E5/*n*-octanol: Role of the alcohol in microemulsions. *J. Phys. Chem.*, **99**, 10313–10318.
13. Schubert, K.-V. and Kaler, E.W. (1996) Non-ionic microemulsions. *Ber. Bunsenges. Phys. Chem.*, **100**, 190–205.
14. Lekkerkerker, H.N.W., Kegel, W.K. and Overbeek, J.Th.G. (1996) Phase behavior of ionic microemulsions. *Ber. Bunsenges. Phys. Chem.*, **100**, 206–217.

15. Aveyard, R., Binks, B.P., Clark, S. and Mead, J. (1986) Interfacial tension minima in oil–water–surfactant systems. *J. Chem. Soc. Faraday Trans.*, **82**, 125–142.
16. Langevin, D. (1992) Low interfacial tensions in microemulsions. In S.H. Chen, J.S. Huang and P. Tartaglia (eds), *Structure and Dynamics of Strongly Interacting Colloids and Supramolecular Aggregates in Solutions*. Kluwer Academic Publishers, Dordrecht, pp. 325–349.
17. Sottmann, T. and Strey, R. (1997) Ultralow interfacial tensions in water–*n*-alkane–surfactant systems. *J. Chem. Phys.*, **106**, 8606–8615.
18. Shinoda, K. and Friberg, S. (1975) Microemulsions – Colloidal aspects. *Adv. Colloid Interface Sci.*, **4**, 281–300.
19. Schechter, R.S., Wade, W.H., Weerasooriya, U., Weerasooriya, V. and Yiv, S. (1985) Synthesis and performance of isomer-free secondary alkane sulfonate surfactants. *J. Dispersion Sci. Techn.*, **6**, 223.
20. Bodet, J.F., Bellare, J.R., Davis, H.T., Scriven, L.E. and Miller, W.G. (1988) Fluid microstructure transition from globular to bicontinuous in midrange microemulsion. *J. Phys. Chem.*, **92**, 1898–1902.
21. Lindman, B., Shinoda, K., Olsson, U., Anderson, D., Karlström, G. and Wennerström, H. (1989) On the demonstration of biconinuous structures in microemulsions. *Colloids Surfaces*, **38**, 205–224.
22. Jahn, W. and Strey, R. (1988) Microstructure of microemulsions by freeze fracture electron microscopy. *J. Phys. Chem.*, **92**, 2294–2301.
23. Lichterfeld, F., Schmeling, T. and Strey, R. (1986) On the microstructure of microemulsions of the system H_2O–*n*-Tetradecane–$C_{12}E_5$. *J. Phys. Chem.*, **90**, 5762–5766.
24. Chen, S.H. (1986) Small angle neutron scattering studies of the structure and interaction in micellar and microemulsions. *Ann. Rev. Phys. Chem.*, **37**, 351–399.
25. Strey, R. (1994) Microemulsion microstructure and interfacial curvature. *Colloid Polym. Sci.*, **272**, 1005.
26. Sottmann, T. and Strey, R. (2005) Microemulsions. In J. Lyklema (ed), *Fundamentals of Interface and Colloid Science*, Vol. V. Academic Press, New York.
27. Jakobs, B., Sottmann, T., Strey, R., Allgaier, J., Willner, L. and Richter, D. (1999) Amphiphilic block copolymers as efficiency boosters for microemulsions. *Langmuir*, **15**, 6707.
28. Jakobs, B., Sottmann, T., Strey, R., Allgaier, J., Willner, L. and Richter, D. (2004) Method for increasing the efficiency of surfactants with simultaneous suppression of lamellar mesophases and surfactants with an additive added thereto. Patent No. US 6,677,293.
29. Bagger-Jörgensen, H., Coppola, L., Thuresson, K., Olsson, U. and Mortensen, K. (1997) Phase behavior, microstructure, and dynamics in a non-ionic microemulsion on addition of hydrophobically end-capped poly(ethylene oxide). *Langmuir*, **13**, 4204–4218.
30. Sassen, C.L., Cassielles, A.G., De Loos, T.W. and De Swaan-Arons, J. (1992) The influence of pressure and temperature on the phase behavior of the system H_2O + C12 + C7E5 and relevant binary subsystems. *Fluid Phase Equilibria*, **72**, 173–187.
31. Laughlin, R.G. (1994) *Aqueous Phase Behavior of Surfactants*. Academic Press, New York.
32. Safran, S.A. (1992) Microemulsions: An ensemble of fluctuating interfaces. In S.-H. Chen, J.S. Huang, P. Tartaglia (eds), *Structure and Dynamics of Strongly Interacting Colloids and Supramolecular Aggregates in Solutions*. Kluwer Academic Publishers, Dordrecht, pp. 237–263.
33. Sottmann, T. (2002) Solubilization efficiency boosting by amphiphilic block copolymers in microemulsions. *Curr. Opin. Coll. Interface Sci.*, **7**, 57–65.
34. Burauer, S., Sachert, T., Sottmann, T. and Strey, R. (1999) On microemulsion phase behavior and the monomeric solubility of surfactant. *Phys. Chem. Chem. Phys.*, **1**, 4299–4306.
35. Lade, O., Beizai, K., Sottmann, T. and Strey, R. (2000) Polymerizable non-ionic microemulsions: Phase behavior of H_2O–*n*–Alkyl Methacrylate–*n*–Alkyl Poly Ethylenglycol Ether (C_iE_j). *Langmuir*, **16**, 4122–4130.

36. Engelskirchen, S., Elsner, N., Sottmann, T. and Strey, R. (2007) Triacylglycerol microemulsions stabilized by alkyl ethoxylate surfactants – A basic study: Phase behaviour, interfacial tensions and microstructure. *J. Colloid Interface Sci.*, **312**, 114–121.
37. Kahlweit, M., Strey, R. and Busse, G. (1990) Microemulsions – A qualitative thermodynamic approach. *J. Phys. Chem.*, **94**, 3881.
38. Burauer, S., Sottmann, T. and Strey, R. (2000) Non-ionic microemulsions with cyclic oils – Oil penetration, efficiency and monomeric solubility. *Tenside Surfactants Detergents*, **37**, 8–16.
39. Kunieda, H. and Shinoda, K. (1985) Evaluation of the hydrophile–lipophile balance (HLB) of non-ionic surfactants. 1. Multisurfactant mixtures. *J. Colloid Interface Sci.*, **107**, 107–121.
40. Kahlweit, M., Strey, R. and Firman, P. (1986) Search for tricritical points in ternary systems: Water–oil–non-ionic amphiphile. *J. Phys. Chem.*, **90**, 671.
41. Kahlweit, M., Strey, R. and Busse, G. (1993) Weakly to strongly structured mixtures. *Phys. Rev. E*, **47**, 4197–4209.
42. De Gennes, P.G. and Taupin, C. (1982) Microemulsions and the flexibility of oil/water interfaces. *J. Phys. Chem.*, **86**, 2294–2304.
43. Debye, P., Anderson, H.R. and Brumberger, H. (1957) Scattering by an inhomogeneous solid. 2. The correlation function and its application. *J. Appl. Phys.*, **28**, 679–683.
44. Talmon, Y. and Prager, S. (1978) Statistical thermodynamics of phase-equilibria in microemulsions. *J. Chem. Phys.*, **69**, 2984–2991.
45. Volmer, M. (1927) Zur Theorie der lyophilen Kolloide. *Z. Phys. Chem.*, **125**, 151–157.
46. Volmer, M. (1957) Die kolloidale Natur von Flüssigkeitsgemischen in der Umgebung des kritischen Lösungspunktes I. *Z. Phys. Chem.*, **206**, 181–193.
47. Sottmann, T. and Strey, R. (1996) Evidence of corresponding states in ternary microemulsions of water–alkane–CiEj. *J. Phys. Condens. Matter*, **8**, A39.
48. Kilpatrick, P.K., Gorman, C.A., Davis, H.T., Scriven, L.E. and Miller, W.G. (1986) Patterns of phase-behavior in ternary ethoxylated alcohol–normal alkane–water mixtures. *J. Phys. Chem.*, **90**, 5292–5299.
49. Strey, R. (1996) Water–non-ionic surfactant systems, and the effect of additives. *Ber. Bunsenges. Phys. Chem.*, **100**, 182.
50. Tlusty, T., Safran, S.A., Menes, R. and Strey, R. (1997) Scaling laws for microemulsions governed by spontaneous curvature. *Phys. Rev. Lett.*, **78**, 2616–2619.
51. Tlusty, T., Safran, S.A. and Strey, R. (2000) Topology, phase instabilities, and wetting of microemulsion networks. *Phys. Rev. Lett.*, **84**, 1244–1247.
52. Zilman, A.G. and Safran, S.A. (2002) Thermodynamics and structure of self-assembled networks. *Phys. Rev. E*, **66**, 051107.
53. Graciaa, A., Lachaise, J., Sayous, J.G., Grenier, P., Yiv, S., Schechter, R.S. and Wade, W.H. (1983) The partitioning of complex surfactant mixtures between oil–water microemulsion phases at high surfactant concentrations. *J. Colloid Interface Sci.*, **93**, 474–486.
54. Kunieda, H. and Ishikawa, N. (1985) Evaluation of the hydrophile lipophile balance (HLB) of non-ionic surfactants. 2. Commercial surfactant systems. *J. Colloid Interface Sci.*, **1985**, 122–128.
55. Sottmann, T., Lade, M., Stolz, M. and Schomäcker, R. (2002) Phase behavior of non-ionic microemulsions prepared from technical-grade surfactants. *Tenside Surf. Det.*, **39**, 20–28.
56. Jakobs, B., Sottmann, T. and Strey, R. (2000) Efficiency boosting with amphiphilic block copolymers – a new approach to microemulsion formulation. *Tenside Surf. Det.*, **37**, 357–364.
57. Stubenrauch, C. (2001) Sugar surfactants – aggregation, interfacial and adsorption phenomena. *Curr. Opin. Coll. Interface Sci.*, **6**, 160–170.
58. Fukuda, K., Söderman, O., Lindman, B. and Shinoda, K. (1993) Microemulsions formed by alkyl polyglycosides an alkyl glycerol ether. *Langmuir*, **9**, 2921–2925.

59. Kahlweit, M., Busse, G. and Faulhaber, B. (1995) Preparing microemulsions with alkyl monoglycosides and the role of *n*-alkanols. *Langmuir*, **11**, 3382–3387.
60. Stubenrauch, C., Paeplow, B. and Findenegg, G.H. (1997) Microemulsions formed by octyl monglycoside and geraniol. Part 1: The role of the alcohol in the interfacial layer. *Langmuir*, **13**, 3652–3658.
61. Sottmann, T., Kluge, K., Strey, R., Reimer, J. and Söderman, O. (2002) General patterns of the phase behavior of mixtures of H_2O, alkanes, alkyl glucosides, and cosurfactants. *Langmuir*, **18**, 3058–3067.
62. Ryan, L.D., Schubert, K.-V. and Kaler, E.W. (1997) Phase behavior of microemulsions made with *n*-alkyl monoglucosides and *n*-alkyl polyglycol ethers. *Langmuir*, **13**, 1510–1518.
63. Kunieda, H. and Yamagata, M. (1993) Mixing of non-ionic surfactants at water oil interfaces in microemulions. *Langmuir*, **9**, 3345–3351.
64. Yamaguchi, S. and Kunieda, H. (1997) Determination of a three-phase tie triangle (the hydrophile-lipophile balance plane) in a composition tetrahedron: Evaluation of the composition of adsorbed mixed-surfactant and the monomeric solubilities of short-chain surfactant. *Langmuir*, **13**, 6995–7002.
65. Billman, J.F. and Kaler, E.W. (1990) Structure and phase-behavior in 5-component microemulsions. *Langmuir*, **6**, 611–620.
66. Lekkerkerker, H.N.W., Kegel, W.K. and Overbeek, J.T.G. (1996) Phase behavior of ionic microemulsions. *Ber. Bunsenges. Phys. Chem.*, **100**, 206–217.
67. Kahlweit, M., Strey, R., Schomäcker, R. and Haase, D. (1989) General patterns of the phase behavior of mixtures of H_2O, nonpolar solvents, amphiphiles, and electrolytes. 2. *Langmuir*, **5**, 305–315.
68. Chen, S.J., Evans, D.F. and Ninham, B.W. (1984) Properties and structure of 3-component ionic microemulsions. *J. Phys. Chem.*, **88**, 1631–1634.
69. Chen, S.H., Chang, S.-L. and Strey, R. (1990) Structural evolution within the one-phase region of a three-component microemulsion: Water-*n*-decane-sodium-bis-ethylhexylsulfosuccinate (AOT). *J. Chem. Phys.*, **93**, 1907–1918.
70. Wade, W.H., Morgan, J.C., Schechter, R.S., Jacobson, J.K. and Salager, J.L. (1978) Interfacial tension and phase behavior of surfactant systems. *Soc. Petroleum Eng.*, **18**, 242–252.
71. Kahlweit, M., Strey, R., Haase, D. and Firman, P. (1988) Properties of the three-phase bodies in H_2O-oil-non-ionic amphiphile mixtures. *Langmuir*, **4**, 785–790.
72. Prince, L.M. (1977) *Microemulsions: Theory and Practice*. Academic Press, New York.
73. Schwuger, M.-J., Stickdorn, K. and Schomäcker, R. (1995) Microemulsions in technical processes. *Chem. Rev.*, **95**, 849–864.
74. Ambwani, D.S. and Fort, T. (1979) Pendant drop technique for measuring liquid boundary tensions. In R.J Good and R.R Stromberg (eds), *Surface and Colloid Science*, Vol. II. Plenum, New York.
75. Langevin, D. and Meunier, J. (1977) Light scattering by liquid interfaces. In H.Z. Cummins and P. Pike (eds), *Photon Correlation Spectroscopy and Velocimetry*, Plenum, New York.
76. Vonnegut, B. (1942) Rotating bubble method for the determination of surface and interfacial tensions. *Rev. Sci. Instr.*, **13**, 6–9.
77. Gibbs, J.W. (1928) *The Collected Works of J.W. Gibbs*, Vol. 1. Longmans Green, London.
78. Aveyard, R., Binks, B.P. and Fletcher, P.D.I. (1990) Surfactant molecular geometry within planar and curved monolayers in relation to the microemulsion phase behavior. In D.M. Bloor and E. Wyn-Jones (eds), *The Structure, Dynamics and Equilibrium Properties of Colloidal Systems*. Kluwer Academic Publishers, Dordrecht/Boston/London, pp. 557–581.
79. Rosen, M.J. and Murphy, D.S. (1991) Effect of the nonaqueos phase on interfacial properties of surfactants. 2. Individual and mixed non-ionic surfactants in hydrocarbon/water systems. *Langmuir*, **7**, 2630–2635.

80. Sottmann, T., Strey, R. and Chen, S.H. (1997) A SANS study of non-ionic surfactant molecules at the water–oil interface: Area per molecule, microemulsion domain size and rigidity. *J. Chem. Phys.*, **106**, 6483.
81. Lang, J.C. and Widom, B. (1975) Equilibrium of 3 liquid-phases and approach to tricritical point in benzene–ethanol–water ammonium sulfate mixtures. *Physica A*, **81**, 190–213.
82. Cazabat, A.M., Langevin, D., Meunier, J. and Pouchelon, A. (1982) Critical-behavior in microemulsions. *J. Phys. Lett.*, **43**, L89–L95.
83. Widom, B. (1987) Phase-transitions in surfactant solutions and in their interfaces. *Langmuir*, **3**, 12–17.
84. Fletcher, P.D.I. and Horsup, D.I. (1992) Droplet dynamics in water-in-oil microemulsions and macroemulsions stabilized by non-ionic surfactants – correlation of measured rates with monolayer bending elasticity. *J. Chem. Soc. Faraday Trans.*, **88**, 855–864.
85. Bonkhoff, K., Hirtz, A. and Findenegg, G.H. (1991) Interfacial-tensions in the three-phase region of non-ionic surfactant + water + alkane systems – critical point effects and aggregation behavior. *Physica A*, **172**, 174–199.
86. Schubert, K.-V., Strey, R., Kline, S. and Kaler, E.W. (1994) Small-angle neutron scattering near the Lifshitz lines: Transition from weakly structured mixtures to microemulsions. *J. Chem. Phys.*, **101**, 5343–5355.
87. Kahlweit, M., Jen, J. and Busse, G. (1992) On the stability of microemulsions. 2. *J. Chem. Phys.*, **97**, 6917–6924.
88. Lee, L.T., Langevin, D., Meunier, J., Wong, K. and Cabane, B. (1990) Film bending elasticity in microemulsions made with non-ionic surfactants. *Progr. Colloid Polym. Sci.*, **81**, 209–214.
89. Binks, B.P., Meunier, J., Abillon, O. and Langevin, D. (1989) Measurement of film rigidity and interfacial tensions in several ionic surfactant-oil-water microemulsions. *Langmuir*, **5**, 415–421.
90. Kluge, K., Stubenrauch, C., Sottmann, T. and Strey, R. (2001) Temperature-insensitive microemulsions formulated from octyl monoglucoside and alcohols: Potential candidates for applications. *Tenside Surf. Det.*, **38**, 30–40.
91. Leitao, H., Somoza, A.M., Telo da Gama, M.M., Sottmann, T. and Strey, R. (1996) Scaling of the interfacial tension of microemulsions: A phenomenological description. *J. Chem. Phys.*, **105**, 2875–2883.
92. Helfrich, W. (1973) Elastic properties of lipid bilayers – theory and possible experiments. *Z. Naturforsch.*, **28c**, 693.
93. Safran, S.A. and Tlusty, T. (1996) Curvature elasticity models of microemulsions. *Ber. Bunsenges. Phys. Chem.*, **100**, 252–263.
94. Morse, D.C. (1997) Entropy and fluctuation of monolayers, membranes, and microemulsions. *Curr. Opin. Coll. Interface Sci.*, **2**, 365–372.
95. Gompper, G. and Schick, M. (1994) *Self-assembling Amphiphilic Systems*. Academic Press, New York.
96. Leitao, H., Telo da Gama, M.M. and Strey, R. (1998) Scaling of the interfacial tension of microemulsions: A Landau theory approach. *J. Chem. Phys.*, **108**, 4189.
97. Kahlweit, M. and Reiss, H. (1991) On the stability of Microemulsions. *Langmuir*, **7**, 2928–2933.
98. Scriven, L.E. (1976) Equilibrium bicontinuous structure. *Nature*, **263**, 123–125.
99. Jahn, W and Strey, R. (1987) Images of bicontinuous microemulsions by freeze fracture electron microscopy. In J. Meunier, D. Langevin and N. Boccara (eds), *Physics of Amphiphilic Layers*. Springer, Berlin, Heidelberg, p. 353.
100. Benson, H.L., Cox, K.R. and Zweig, J.E. (1985) *Happi*, 50.
101. Kahlweit, M., Strey, R. (1987) Phase behaviour of H_2O–oil–non–ionic amphiphile ternary systems. In M. Clausse (ed), *Microemulsions*, Vol. 24. Marcel Dekker, New York, p. 1.
102. Bowcott, J.E. and Schulman, J.H. (1955) Emulsions – control of droplet size and phase continuity in transparent oil–water dispersions stabilized with soap and alcohol. *Z. Elektrochem.*, **59**, 283.

103. Reimer, J., Söderman, O., Sottmann, T., Kluge, K. and Strey, R. (2003) Microstructure of alkyl glucoside microemulsion: Control of curvature by interfacial composition. *Langmuir*, **19**, 10692–10702.
104. Talmon, Y. (1999) Cryogenic temperature transmission electron microscopy in the study of surfactant systems. In B.P. Binks (ed), *Modern Characterization Methods of Surfactant Systems*. Marcel Dekker, New York, pp. 147–178.
105. Belkoura, L., Stubenrauch, C. and Strey, R. (2004) Freeze fracture direct imaging: A hybrid method in preparing specimen for Cryo-TEM. *Langmuir*, **20**, 4391–4399.
106. Glatter, O. (1982) Data treatment. In O. Glatter and O. Kratky (eds), *Small Angle X-ray Scattering*. Academic Press, London, pp. 119–163.
107. Chu, B. (1974) *Laser Light Scattering*. Academic Press, New York.
108. Berne, B.J. and Pecora, R. (1996) *Dynamic Light Scattering*. Wiley, New York.
109. Lindman, B. and Olsson, U. (1996) Structure of microemulsions studied by NMR. *Ber. Bunsenges. Phys. Chem.*, **100**, 344–363.
110. Eicke, H.F., Shepherd, J.C.W. and Steinmann, A. (1976) Exchange of solubilized water and aqueous-electrolyte solutions between micelles in apolar media. *J. Colloid Interface Sci.*, **56**, 168–176.
111. Burauer, S. (2002) *Elektronenmikroskopie Komplexer Fluide*. TENEA, Berlin.
112. Burauer, S., Belkoura, L., Stubenrauch, C. and Strey, R. (2003) Bicontinuous microemulsions revisited: A new approach to freeze fracture electron microscopy (FFEM). *Colloids Surf. A*, 159–170.
113. Shinoda, K. and Saito, H. (1968) The effect of temperature on phase equilibria and the types of dispersions of the ternary system composed of water, cyclohexane, and non-ionic amphiphile. *J. Colloid Interface Sci.*, **26**, 70–74.
114. Kahlweit, M., Strey, R. and Schomäcker, R. (1989) Microemulsions as liquid media for chemical reactions. In W. Knoche and R. Schomäcker (eds), *Reactions in Compartmentalized Liquids*. Springer, Berlin, Heidelberg, pp. 1–10.
115. Kahlweit, M., Strey, R., Haase, D., Kunieda, H., Schmeling, T., Faulhaber, B., Borkovec, M., Eicke, H.F., Busse, G., Eggers, F., Funck, T., Richmann, H., Magid, L., Söderman, O., Stilbs, P., Winkler, J., Dittrich, A. and Jahn, W. (1987) How to study microemulsions. *J. Colloid Interface Sci.*, **118**, 436–453.